bioRxiv preprint doi: https://doi.org/10.1101/2021.06.04.447151; this version posted June 7, 2022. The copyright holder for this preprint (which was not certified by peer review) is the author/funder, who has granted bioRxiv a license to display the preprint in perpetuity. It is made available under aCC-BY-NC-ND 4.0 International license.

# TITLE

Single-cell intracellular pH dynamics regulate the cell cycle by timing G1 exit and the G2 transition

# AUTHORS AND AFFILIATIONS

Julia S. Spear[1,2] and Katharine A. White[1,2]

[1]Department of Chemistry and Biochemistry, University of Notre Dame, Notre Dame, IN, USA

[2]Harper Cancer Research Institute, University of Notre Dame, Notre Dame, IN, USA

*To whom correspondence should be addressed: kwhite6@nd.edu

## SUMMARY

Spear et al. characterize an approach for measuring single-cell intracellular pH (pHi) and monitoring single-cell pHi dynamics during cell cycle progression. By tracking pHi in single cells, Spear et al. confirm prior work at the population level showing an increase in pHi at the G2/M transition. However, single-cell pHi measurements reveal new features of pHi dynamics during cell cycle progression, including significantly decreased pHi at the G1/S boundary, S/G2 boundary, and just prior to division, and increases during mid-S phase and G2. Using pHi manipulation, Spear et al. determine that decreased pHi shortens G1 phase and increased pHi elongates G1 phase, indicating low pHi is a cue for G1 exit. S phase progression was also reliant on temporal pHi changes, suggesting pHi dynamics are necessary for cell cycle progression.

## ABSTRACT (160 words)

Transient changes in intracellular pH (pHi) regulate normal cell behaviors like migration and proliferation, while pHi dynamics are dysregulated in cancer. However, it is unclear how spatiotemporal pHi dynamics influence single-cell behaviors. We performed single-cell pHi measurements in normal and cancer cell lines and measured spatiotemporal pHi dynamics during cell cycle progression. Single-cell pHi is dynamic (0.16±0.07 pH units) throughout the cell cycle, with decreased pHi at G1/S, late S, and mitosis and increased pHi in mid-S and G2/M. We next experimentally manipulated pHi and measured effects on cell cycle progression. We show that decreased pHi is a permissive cue for G1 exit, with decreased pHi shortening G1 and increased pHi elongating G1. We also show that dynamic pHi is required for S phase timing, as high pHi elongates S phase and low pHi inhibits S/G2 transition. This work shows dynamic pHi is necessary for cell cycle progression in single cells.

bioRxiv preprint doi: https://doi.org/10.1101/2021.06.04.447151; this version posted June 7, 2022. The copyright holder for this preprint (which was not certified by peer review) is the author/funder, who has granted bioRxiv a license to display the preprint in perpetuity. It is made available under aCC-BY-NC-ND 4.0 International license.

## INTRODUCTION

In normal cells, intracellular pH (pHi) is near neutral (~7.2) while extracellular pH (pHe) is more alkaline (~7.4). Transient changes in pHi driven by ion transporter activity (Boron, 2004) have been shown to regulate normal cell behaviors such as differentiation (Ulmschneider et al., 2016), proliferation (Flinck et al., 2018a), migration (Martin et al., 2011a)(Choi et al., 2013), and apoptosis (Sergeeva et al., 2017). However, most studies of pHi-dependent cell behaviors measure average pHi across a population of cells and perform pHi measurements in non-native cellular environments. Thus, our understanding of the role of spatiotemporal and single-cell pHi dynamics in regulating cell behaviors is limited. Understanding how spatiotemporal pHi dynamics drive single-cell behaviors like division, migration, and apoptosis would enhance mechanistic understanding of pHi dynamics in biology. In addition, a mechanistic understanding of pHi dynamics could lead to new therapeutic routes for limiting pHi-dependent behaviors in diseases with dysregulated pHi, such as cancer (White et al., 2017a; Harguindey et al., 2017) and neurodegeneration (Majdi et al., 2016).

Previous work characterizing single-cell pHi in 2D cell cultures has suggested pHi is heterogeneous (Korenchan and Flavell, 2019). Mouse and human cancer cells were shown to have a distribution of fluorescence ratios when calculated by fluorescence-activated cell sorting (FACS) using the pH-sensitive dye 2',7'-bis(carboxyethyl)-5(6)-Carboxyfluorescein (BCECF) (Lee and Tannock, 1998). This suggests that single-cell pHi is heterogeneous in 2D cell cultures, but the dye was not standardized on the single-cell

bioRxiv preprint doi: https://doi.org/10.1101/2021.06.04.447151; this version posted June 7, 2022. The copyright holder for this preprint (which was not certified by peer review) is the author/funder, who has granted bioRxiv a license to display the preprint in perpetuity. It is made available under aCC-BY-NC-ND 4.0 International license.

level and therefore absolute pHi calculations were not possible. Another limitation of this work is that pHi can be rapidly altered when the cells are trypsinized for FACS analysis, as many ion transporters are also mechanosensitive (Barth and Fronius, 2019; Fuster et al., 2004). In another study using a small number (n<150) of normal and cancerous mouse mammary cells, heterogeneous pHi was linked to metabolic changes (Warburg-like metabolism vs. oxidative phosphorylation) (Lobo et al., 2016). However, the authors did not confirm that single-cell pHi correlated with single-cell metabolic phenotypes. Collectively, these data suggest that single-cell pHi may be heterogeneous in these models and that pHi may report on phenotype or cell state. Unfortunately, the lack of single-cell correlations and the use of non-native environments limit the interpretation of these data.

One pHi-dependent behavior that would benefit significantly from more rigorous single-cell pHi measurements and characterization is proliferation. Cell division is fundamentally a single-cell behavior, but previous studies of cell cycle progression and pHi have been performed at the population level using non-native environments (Taylor and Hodson, 1984; Flinck et al., 2018b; Putney and Barber, 2003) or using lower order organisms (Gillies and Deamer, 1979; Aerts et al., 1985; Karagiannis and Young, 2001).

The first experiments identifying a relationship between cell cycle and pHi used unicellular organisms, such as tetrahymena (Gillies and Deamer, 1979), *Dictyostelium* (Aerts et al., 1985), and *S. pombe* (Karagiannis and Young, 2001). In tetrahymena, two increases in pHi (0.4 pH units) were observed pre- and post-S phase (Gillies and Deamer, 1979).

bioRxiv preprint doi: https://doi.org/10.1101/2021.06.04.447151; this version posted June 7, 2022. The copyright holder for this preprint (which was not certified by peer review) is the author/funder, who has granted bioRxiv a license to display the preprint in perpetuity. It is made available under aCC-BY-NC-ND 4.0 International license.

However, all pHi changes were measured at the population level and used harsh synchronization techniques (starvation and heat shock) that disrupt essential cell metabolic functions. In *Dictyostelium*, increased pHi (~0.2 pH units) was measured during S phase and when pHi was artificially increased, DNA replication and protein synthesis were increased as well (Aerts et al., 1985). This indicates that high pHi may drive S phase progression and S phase-related cell functions. However, no timing or delays in S phase progression were noted and only population-level pHi measurements were made. In conflict with the two previous studies, no evidence was found for a relationship between cell cycle and pHi in *S. pombe* using a genetically-encoded pHi biosensor (pHluorin) (Karagiannis and Young, 2001). Thus, the existing data in unicellular organisms is inconsistent in whether pHi regulates (or times) cell cycle progression.

While some essential cell functions are evolutionarily conserved, pHi fluctuations in unicellular organisms may not be recapitulated in multicellular models. However, some studies in animal cell models have also shown a relationship between pHi and cell cycle progression. In quiescent populations of human tumor cells, it was shown that a narrow range of pHe values (pH 6.8 to 7.2) can recruit cells into the cell cycle (Taylor and Hodson, 1984). This suggests that a defined range of pHe is required for normal proliferation, but they did not measure pHi which can be altered in response to pHe changes (Deutsch et al., 1982). In population-level analyses of pHi in thymidine-synchronized MCF-7 breast cancer cells, pHi was found to fluctuate after thymidine release but no statistical significance was noted (Flinck et al., 2018b). Strengthening the link between pHi and cell cycle regulation, knockdown of the $Na^+/H^+$ exchanger (NHE1) and $Na^+$-$HCO_3^-$ transporter (NBCn1) caused elongation of S phase and a delay in the G2/M transition (Flinck et al.,

bioRxiv preprint doi: https://doi.org/10.1101/2021.06.04.447151; this version posted June 7, 2022. The copyright holder for this preprint (which was not certified by peer review) is the author/funder, who has granted bioRxiv a license to display the preprint in perpetuity. It is made available under aCC-BY-NC-ND 4.0 International license.

2018b), but no single-cell pHi measurements were made. In another example, an increase in pHi driven by NHE1 was found to time the G2/M transition (Putney and Barber, 2003). However, the experiments in these studies were carried out using population-level assays and performed using environmental (pHe) changes or genetic ion transporter knockdown. As ion transporters also serve scaffolding and signaling roles, knockdown can produce transport-independent effects on cell biology. Although these studies lay a framework for a relationship between pHi and cell cycle, there is a need for single-cell pHi measurements in native environments to elucidate how temporal pHi dynamics regulate cell cycle progression.

Here, we present single-cell pHi measurements under physiological conditions in both asynchronous and synchronized cell populations to determine if pHi regulates cell cycle progression at the single-cell level. First, we show that asynchronous lung cancer cells have increased pHi compared to lung epithelial cells and the pHi distributions were similar between all cell populations. To investigate pHi during specific cell cycle phases, we synchronized cells in G1 (Palbociclib) and early S phase (thymidine) and measured pHi as cells were released using endpoint and time-lapse microscopy. We determined that single-cell pHi oscillated during cell cycle progression: pHi significantly decreased at G1/S, S/G2, and mitosis, and increased during mid-S and G2/M. Using pHi manipulation and Fluorescent Ubiquitination-based Cell Cycle Indicator (FUCCI) reporters, we determined dynamic pHi is necessary for normal progression through the cell cycle. We show that low pHi is a cue for G1 exit and normal S phase duration requires both a pHi increase and decrease. This work highlights the advantages of using single-cell pHi

bioRxiv preprint doi: https://doi.org/10.1101/2021.06.04.447151; this version posted June 7, 2022. The copyright holder for this preprint (which was not certified by peer review) is the author/funder, who has granted bioRxiv a license to display the preprint in perpetuity. It is made available under aCC-BY-NC-ND 4.0 International license.

measurements to investigate single-cell behaviors like cell cycle, as we show previously uncharacterized pHi dynamics regulating G1 exit and S phase.

## RESULTS

### Single-cell pHi in asynchronous cell populations is heterogenous, but is increased in transformed and metastatic lung cells compared to normal cells

In normal epithelial cells, pHi is near neutral (~7.2), while cancer cells have a constitutively increased pHi (pHi>7.4). This constitutively increased pHi occurs early in cancer development (Reshkin et al., 2000; Cardone et al., 2005) and promotes pHi-dependent behaviors such as proliferation, cell invasion, and metastasis (White et al., 2017a). Our first goal was to determine if we could accurately quantify single-cell pHi distributions within various clonal lung cell lines (normal and cancerous). We used a genetically-encoded biosensor, mCherry-pHluorin (mCh-pHl), for our applications (Koivusalo et al., 2010). The mCh-pHl biosensor has been used to measure pHi in cultured cells (Koivusalo et al., 2010; Choi et al., 2013) and tissues (Grillo-Hill et al., 2015) and has a dynamic linear range between pH 6.5 and 8.0 (Grillo-Hill et al., 2014). Briefly, direct measurement of pHi in single living cells can be achieved by performing ratiometric imaging of pHluorin/mCherry fluorescence intensities. Fluorescence of pHluorin is pH-sensitive in the physiological range while mCherry fluorescence is not and can be used to normalize biosensor expression. At the end of the experiments, single-cell standardization is performed using buffers of known pH containing the protonophore nigericin (Fig. 1A, see methods for details). This method of pHi measurement avoids issues of uneven dye

bioRxiv preprint doi: https://doi.org/10.1101/2021.06.04.447151; this version posted June 7, 2022. The copyright holder for this preprint (which was not certified by peer review) is the author/funder, who has granted bioRxiv a license to display the preprint in perpetuity. It is made available under aCC-BY-NC-ND 4.0 International license.

loading, washout, and photobleaching that are associated with pH-sensitive dyes (Grillo-Hill et al., 2014).

We first examined whether asynchronous single-cell pHi measurements under physiological conditions could recapitulate population-level averages while also reflecting physiological heterogeneity. We stably expressed mCh-pHl in normal lung epithelial cells (NL20), primary tumor site-derived lung cancer cells (A549), and metastatic site-derived lung cancer cells (H1299). We confirmed that population pHi measurements in the clonal biosensor lines (NL20-mCh-pHl, A549-mCh-pHl and H1299-mCh-pHl) were unchanged compared to matched parental cell lines using a standard plate reader assay with the pH-sensitive dye BCECF (Grillo-Hill et al., 2014) (Fig. S1). We next measured single-cell pHi in individual NL20-mCh-pHl (Fig. 1B), A549-mCh-pHl (Fig. 1C), and H1299-mCh-pHl (Fig. 1D) cells. Representative pHluorin and mCherry channels and single-cell standardization lines can be found in Fig. S2. To quantify heterogeneity in these clonal cell lines, we prepared distribution histograms of single-cell pHi measurements. We found that the pHi of primary tumor cells (A549-mCh-pHl) (Fig. 1F; 7.54±0.07) was increased compared to normal lung epithelial cells (NL20-mCh-pHl) (Fig. 1E; 7.42±0.07). Importantly, metastatic tumor cells (H1299-mCh-pHl) had the highest median pHi (Fig. 1G; 7.65±0.07), which was significantly higher than both the normal and primary tumor clonal cell lines. These data show the advantages of measuring single-cell pHi under physiological culture conditions that match population averages, but also provide pHi distributions lost at the population level. These data also show that pHi is heterogeneous even in clonal,

bioRxiv preprint doi: https://doi.org/10.1101/2021.06.04.447151; this version posted June 7, 2022. The copyright holder for this preprint (which was not certified by peer review) is the author/funder, who has granted bioRxiv a license to display the preprint in perpetuity. It is made available under aCC-BY-NC-ND 4.0 International license.

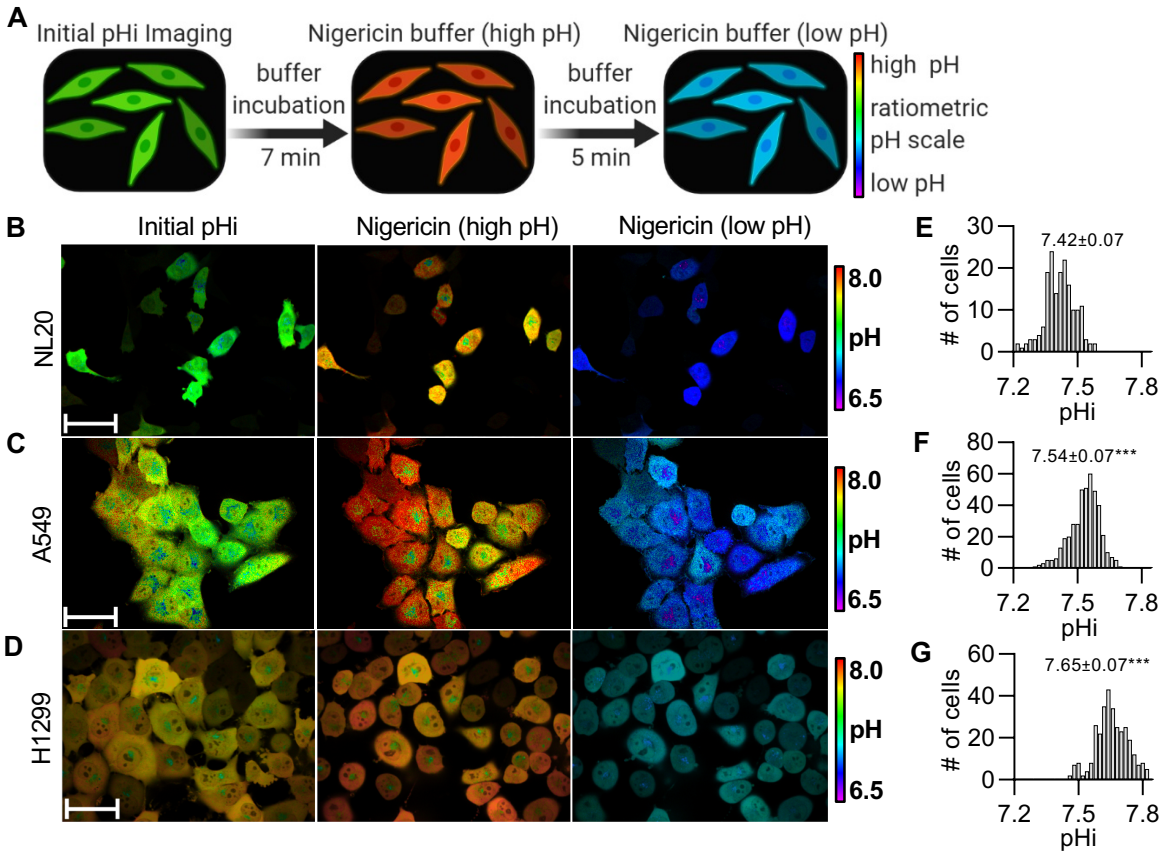


175 genetically identical, cell lines, suggesting pHi may be a biomarker for non-genetic cell

176 phenotype.

177

178

179 **Figure 1: Intracellular pH is heterogeneous in normal and cancerous lung cell lines**
180 **and median pHi significantly increases in cancer cells.**
181 A) Schematic of single-cell pHi measurements using a stably expressed pH biosensor,
182 mCherry-pHluorin (mCh-pHl), and the protonophore nigericin to standardize the
183 biosensor (see methods for details). B-D) Representative images of pHi measurements
184 and standardization in B) NL20, C) A549, and D) H1299 cells stably expressing mCh-pHl.
185 Ratiometric display of pHluorin/mCherry fluorescence ratios, scale bars: 50 μm. E-G)
186 Histograms of single-cell pHi in E) NL20 (n=173, 3 biological replicates), F) A549 (n=424,
187 4 biological replicates), and G) H1299 (n=315, 3 biological replicates). Histograms are
188 binned at 0.02 pH units. Above histograms, median±S.D. Significance was determined
189 by a Mann Whitney test. (***p<0.001, compared to NL20).
190

bioRxiv preprint doi: https://doi.org/10.1101/2021.06.04.447151; this version posted June 7, 2022. The copyright holder for this preprint (which was not certified by peer review) is the author/funder, who has granted bioRxiv a license to display the preprint in perpetuity. It is made available under aCC-BY-NC-ND 4.0 International license.

From our data, we measured a range of pHi values within single distributions of clonal cell lines, suggesting pHi heterogeneity may reflect non-genetic, phenotypic heterogeneity. We noted that the single-cell pHi measurements were performed in asynchronous cell populations (Fig. 1) and prior work suggests pHi is dynamic during the mammalian cell cycle (Putney and Barber, 2003; Flinck et al., 2018b). However, those experiments were performed at the population level and used non-physiological environments (FACS) that can produce artifactual effects on pHi. With our ability to measure single-cell pHi in physiological environments, we sought to measure pHi dynamics during cell cycle phases and characterize the regulatory effect of pHi on cell cycle progression in single cells.

**Cells released from G1 synchronization have dynamic pHi**

Using mCh-pHl and cell synchronization methods, we measured single-cell pHi dynamics during cell cycle progression. We synchronized H1299-mCh-pHl cells using Palbociclib, which blocks the phosphorylation of the retinoblastoma protein and synchronizes cells prior to the G1 checkpoint (Liu et al., 2018) (Fig. 2A). It has recently been shown that Palbociclib is an efficient G1 synchronizer in H1299 cells, with nearly 85% synchronization after 24 h treatment and minimal DNA damage (Trotter and Hagan, 2020). After synchronization (0.1 μM Palbociclib), cells were imaged at 0, 4, 8, 12, 24, and 36 hours (h) after release (Fig. 2B) and single-cell pHi distributions were measured (Fig. 2C). Qualitatively, we noticed cells were larger at earlier time points (0-4 h) and starting at 12 h cells exhibited altered morphology that could indicate mitosis (Fig. 2B). Through ratiometric imaging, we found cells had low pHi from 4-8 h and high pHi at 24 h

bioRxiv preprint doi: https://doi.org/10.1101/2021.06.04.447151; this version posted June 7, 2022. The copyright holder for this preprint (which was not certified by peer review) is the author/funder, who has granted bioRxiv a license to display the preprint in perpetuity. It is made available under aCC-BY-NC-ND 4.0 International license.

(Fig. 2B). In this representative replicate, we observed single-cell pHi significantly decreased between 0 and 4 h, significantly increased between 4 and 8 h, decreased between 8 and 12 h, and increased again between 12 and 24 h (Fig. 2D). This data suggests that pHi is dynamic during cell cycle progression with multiple fluctuations in pHi after synchronization release.

bioRxiv preprint doi: https://doi.org/10.1101/2021.06.04.447151; this version posted June 7, 2022. The copyright holder for this preprint (which was not certified by peer review) is the author/funder, who has granted bioRxiv a license to display the preprint in perpetuity. It is made available under aCC-BY-NC-ND 4.0 International license.

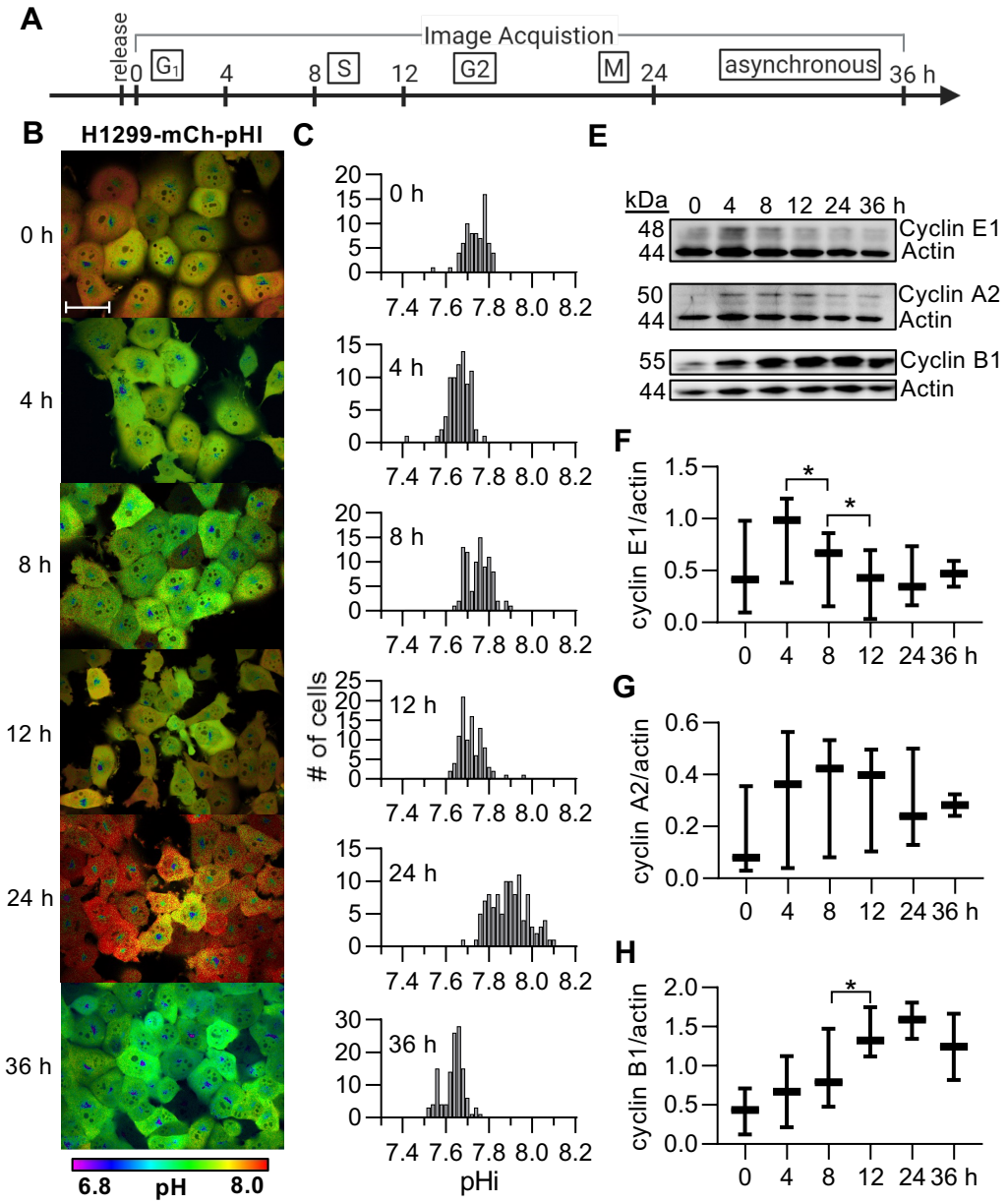


D

| | H1299-mCh-pHI |
|---|---|
| 0 h | 7.75±0.05 |
| 4 h | 7.67±0.04*** |
| 8 h | 7.75±0.05*** |
| 12 h | 7.71±0.05* |
| 24 h | 7.90±0.09*** |
| 36 h | 7.65±0.05*** |

**Figure 2: Intracellular pH is dynamic following G1 synchronization and correlates with cyclin levels.** A) Schematic of image acquisition after Palbociclib synchronization.

bioRxiv preprint doi: https://doi.org/10.1101/2021.06.04.447151; this version posted June 7, 2022. The copyright holder for this preprint (which was not certified by peer review) is the author/funder, who has granted bioRxiv a license to display the preprint in perpetuity. It is made available under aCC-BY-NC-ND 4.0 International license.

B) Representative images of H1299-mCh-pHl cells at indicated time points after release. Ratiometric display of pHluorin/mCherry fluorescence ratios. Scale bar: 50 μm. C) Histograms of single-cell pHi data collected as in B, from one biological replicate. Histograms binned at 0.02 pH units. Additional replicates shown in Fig. S3. D) Medians and standard deviations at each time point shown in C. E) Representative immunoblots for cyclin E1, A2, and B1 with respective actin loading controls. Box and whisker plots of F) cyclin E1, G) cyclin A2, and H) cyclin B1 immunoblot data across 3 biological replicates. Additional replicates shown in Fig. S3. I) Violin plots of raw pHi across 3 biological replicates. In D and I, significance was determined according to a Kruskal Wallis test with Dunn's multiple comparisons correction. In F-H, significance was determined by a paired t-test. In D and F-I, each time point was compared to the preceding time point and in I, 0 h was compared to 24 h. (*$p<0.05$; ***$p<0.001$).

We confirmed that Palbociclib appropriately synchronized the cells by immunoblotting for cyclins from matched cell lysates (Fig. 2E). Cyclin E1 regulates G1/S (Siu et al., 2012), cyclin A2 regulates S and G2 phases (De Boer et al., 2008), while cyclin B1 regulates G2 and is degraded by the start of anaphase in mitosis (Chang et al., 2003). We observe that cyclin E1, a marker of G1/S, significantly increases from 0 to 4 h, which is expected for a cell population properly synchronized in G1 phase (Fig. 2F). These cells undergo mitosis approximately 24 h post-Palbociclib release because cyclin B1 levels, an inducer of G2/M, increased from 8 to 12 h and peaked 24 h post-release (Fig. 2H). By 36 h, protein abundance was similar across all cyclins, as expected in an asynchronous population. Cyclin immunoblots and pHi agreed across 3 biological replicates, and additional blots are shown in Fig. S3. This suggests that our experimental assay using Palbociclib to synchronize cells at G1 is capturing progression through a complete cell cycle.

When pHi measurements on Palbociclib-treated cells were compared over three biological replicates, we found that pHi significantly decreased at the G1/S transition (4 h, 7.75±0.15) and in late S phase (12 h, 7.69±0.09), significantly increased at G2/M (24 h, 7.82±0.11) (Fig. 2I), and then significantly decreased once more at the end of the

bioRxiv preprint doi: https://doi.org/10.1101/2021.06.04.447151; this version posted June 7, 2022. The copyright holder for this preprint (which was not certified by peer review) is the author/funder, who has granted bioRxiv a license to display the preprint in perpetuity. It is made available under aCC-BY-NC-ND 4.0 International license.

experiment in asynchronous cells (36 h, 7.67±0.10) (Fig. 2I). These pooled data recapitulate the wave-like pHi pattern observed in the individual replicate. Individual pHi distribution plots for the additional replicates are shown in Fig. S3. To assess if Palbociclib alters resting pHi on its own, we pooled the synchronized time points (Fig. 2I, 0-24 h) and compared these data to pHi measurements from the endpoint Palbociclib data (Fig. 2I, 36 h) and to untreated, asynchronous H1299-mCh-pHI pHi data (Fig. 1G). Palbociclib-treated cells had a significantly higher pHi than the untreated, asynchronous cells, indicating that Palbociclib synchronization may also alter pHi homeostasis (Fig. S3C). However, this increase in resting pHi is uniform and we are still able to measure significant fluctuations in pHi, with decreasing pHi at G1/S and late S, and increasing pHi leading to G2/M.

**Cells exhibit cell cycle-linked pHi dynamics independent of cell cycle synchronization method**

Because Palbociclib synchronization altered resting pHi (Fig. S3C), we wanted to confirm that the pHi dynamics observed in these experiments were linked to cell cycle phase and not an artifact of the Palbociclib synchronization method. We synchronized H1299-mCh-pHI cells using a double-thymidine block (Chen and Deng, 2018) which halts cells in early S phase. Thymidine acts as a DNA synthesis inhibitor by accumulating dTTP and depleting dCTP within the cell (Bjursell and Reichard, 1973; Bolderson et al., 2004). We synchronized H1299-mCh-pHI cells and imaged them at 0, 4, 8, 12, and 24 h after thymidine release (Fig. 3A-B). Qualitatively, we noticed cells were larger at 0 h and starting at 8 h had distinct cell rounding and smaller apparent cell size that may indicate

bioRxiv preprint doi: https://doi.org/10.1101/2021.06.04.447151; this version posted June 7, 2022. The copyright holder for this preprint (which was not certified by peer review) is the author/funder, who has granted bioRxiv a license to display the preprint in perpetuity. It is made available under aCC-BY-NC-ND 4.0 International license.

mitotic cells (Fig. 3B). In this representative replicate, we observed single-cell pHi significantly decreased between 0 and 4 h, significantly increased between 4 and 8 h, decreased between 8 and 12 h, and increased again between 12 and 24 h (Fig. 3C-D). This general observation supports our data from cells released earlier in the cell cycle (Palbociclib, G1) (Fig. 2) and suggests that pHi is dynamic during the cell cycle regardless of the synchronization method used.

We again confirmed that the treatment appropriately synchronized the cells by immunoblotting for cyclins from matched cell lysates (Fig. 3E). We found that cyclin E1, a marker of G1 and early S phase, is highest at 0 h, as expected for a cell population properly synchronized in early S phase (Fig. 3F). These cells undergo mitosis approximately 8 h after thymidine release because cyclin A2, which is degraded before the G2/M checkpoint, was highest at 4 h and significantly decreased by 8 h, showing transition to late G2 (Fig. 3G). Confirming this, we observed that cyclin B1 levels, an inducer of G2/M, increased from 0 to 4 h and peaked 8 h after release (Fig. 3H). Cyclin E1 levels increased again by 12 h, suggesting most cells in this assay completed the cell cycle and progressed back to G1 phase (Fig. 3F). By 24 h, protein abundance was similar across all cyclins, as we would expect in an asynchronous population. Immunoblots for additional replicates are shown in Fig. S4. These cyclin results match previously published data on synchronized H1299 cell populations (Chen and Deng, 2018), supporting that the thymidine protocol appropriately synchronized the cells.

bioRxiv preprint doi: https://doi.org/10.1101/2021.06.04.447151; this version posted June 7, 2022. The copyright holder for this preprint (which was not certified by peer review) is the author/funder, who has granted bioRxiv a license to display the preprint in perpetuity. It is made available under aCC-BY-NC-ND 4.0 International license.

When pHi was compared over four biological replicates, we found that the median pHi of the cell populations decreased significantly at 4 h (late S phase), increased from 4 to 8 h (G2/M), and decreased once more from 8 to 12 h (M/G1) (Fig. 3I). This preserves the wave-like pHi pattern measured in the individual replicate. Individual pHi distribution plots for additional replicates are shown in Fig. S4. In the merged replicate data, there was no significant difference in pHi between 12 h and 24 h, but at 24 h, pHi was significantly lower than at 0 h (Fig. 3I). Confirming thymidine treatment did not alter pHi, we did not observe any significant differences in pHi when comparing pooled synchronized data (Fig. 3I, 0-12 h) to pHi measurements from both asynchronous thymidine data (Fig. 3I, 24 h) and untreated, asynchronous H1299-mCh-pHI cells (Fig. 1G) (Fig. S4C). Our thymidine pHi data recapitulate both the decreased pHi in late S phase and increased pHi during G2/M that we measured after release from Palbociclib, while also revealing a pHi increase during early S phase.

bioRxiv preprint doi: https://doi.org/10.1101/2021.06.04.447151; this version posted June 7, 2022. The copyright holder for this preprint (which was not certified by peer review) is the author/funder, who has granted bioRxiv a license to display the preprint in perpetuity. It is made available under aCC-BY-NC-ND 4.0 International license.

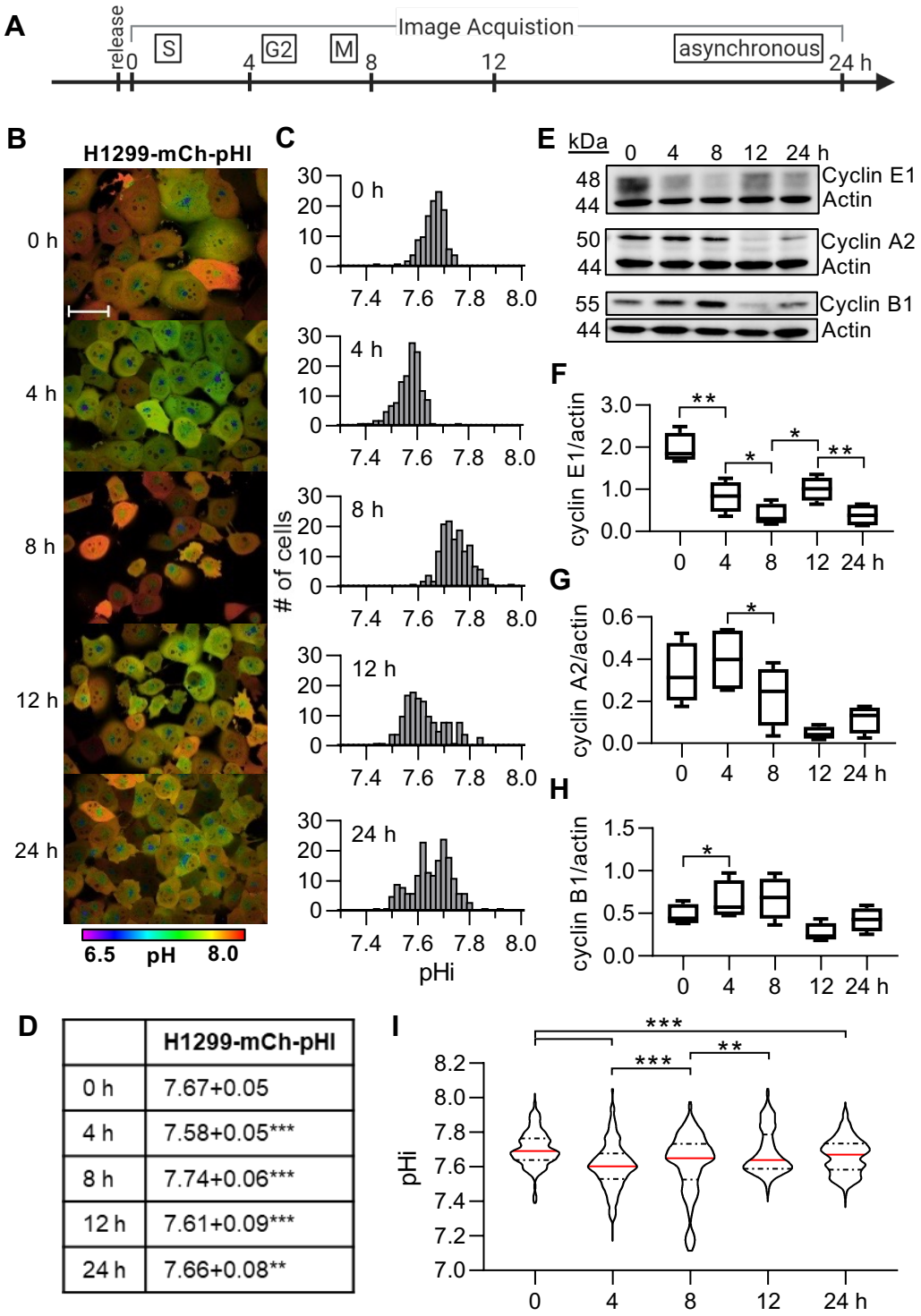


| | H1299-mCh-pHl |
|---|---|
| 0 h | 7.67+0.05 |
| 4 h | 7.58+0.05*** |
| 8 h | 7.74+0.06*** |
| 12 h | 7.61+0.09*** |
| 24 h | 7.66+0.08** |

**Figure 3: Intracellular pH is dynamic after release from early S phase in H1299-mCh-pHl cells and correlates with cyclin levels.**

A) Schematic of image acquisition after a double-thymidine synchronization. B) Representative images of H1299-mCh-pHl cells at indicated time points after release. Ratiometric display of pHluorin/mCherry fluorescence ratios, scale bar: 50 µm. C) Histograms of single-cell pHi data collected in B, from one biological replicate. Histograms

bioRxiv preprint doi: https://doi.org/10.1101/2021.06.04.447151; this version posted June 7, 2022. The copyright holder for this preprint (which was not certified by peer review) is the author/funder, who has granted bioRxiv a license to display the preprint in perpetuity. It is made available under aCC-BY-NC-ND 4.0 International license.

binned at 0.02 pH units. Additional replicates are shown in Fig. S4. D) Table of pHi values from data in C (median±S.D.). E) Representative immunoblots for cyclin E1, A2, and B1 with respective actin loading controls. Box and whisker plots of F) cyclin E1, G) cyclin A2, and H) cyclin B1 immunoblot data across 4 biological replicates. Additional replicates shown in Fig. S4. I) Violin plots of raw pHi across 4 biological replicates. In D and I, significance was determined using a Kruskal Wallis test with Dunn's multiple comparisons correction. In F-H, significance was determined by a paired t-test. In D and F-I, each time point was compared to its preceding time point and in I, 0 h compared to 24 h. (*$p<0.05$; **$p<0.01$; ***$p<0.001$).

To confirm results in H1299-mCh-pHl cells, we similarly synchronized A549-mCh-pHl with a double-thymidine block and observed similar pHi dynamics to H1299-mCh-pHl cells (Fig. S5). Cells were morphologically similar in size to H1299-mCh-pHl populations (Fig. S5A) at respective time points, indicating cell growth leading to mitosis (Fig. S5A; 0-4 h) and mitotic cell rounding during M phase (Fig. S5A; 8 h). The measured pHi values oscillated similarly to H1299-mCh-pHl cells with a decrease from 0 h to 4 h, an increase from 4 h to 8 h, and decreases at 12 h and 24 h (Fig. S5B-C). Again, synchronization by double-thymidine block was confirmed in A549-mCh-pHl cells using cyclin immunoblots, where cyclin A2 (S/G2) peaked at 4 h, cyclin B1 (G2/M) peaked at 8 h, and both proteins were low at 12 h indicating the start of a new cycle with cells in G1 (Fig. S5D). Single-cell pHi distribution plots and western blots for additional replicates are shown in Fig. S6. Like H1299-mCh-pHl cells, collective pHi in A549-mCh-pHl cells across 4 biological replicates significantly increased from 4 h to 8 h (G2/M) and decreased following mitosis at 12 h (Fig. S5E). Observing the same cell-cycle-linked pHi dynamics across different cell models suggests the increases leading to division (G2/M, 4-8 h) and decreases after division (G1, 8-12 h) may be necessary for division timing and re-entry into the cell cycle.

bioRxiv preprint doi: https://doi.org/10.1101/2021.06.04.447151; this version posted June 7, 2022. The copyright holder for this preprint (which was not certified by peer review) is the author/funder, who has granted bioRxiv a license to display the preprint in perpetuity. It is made available under aCC-BY-NC-ND 4.0 International license.

From these varying methods of cell synchronization and combination of pHi endpoint assays through cyclin immunoblots, we conclude that pHi is dynamic through the cell cycle at the single-cell level: pHi decreases during G1/S, increases in early S phase, decreases leading to S/G2, increases prior to G2/M, and drops in pHi following mitosis. While the pHi values are quantified from single-cell measurements, these are endpoint assays with population-level comparisons. We next asked whether pHi dynamics within single, dividing H1299-mCh-pHl cells followed a similar oscillating pHi pattern when tracked over time.

**Single cells alkalize prior to G2/M, followed by rapid acidification during mitosis and pHi recovery in daughter cells**

In the previous experiments, cells from matched populations were identically treated and released from synchronization for sampling at time points after release. Although these time points showed that single-cell pHi distributions fluctuate with cell cycle progression, the snapshots may not reflect continuous single-cell pHi dynamics or single-cell, cell cycle progression phenotypes. To address this limitation, we established a time-lapse approach to track pHi dynamics over an entire cell cycle in a single cell.

We synchronized H1299-mCh-pHl cells with a double thymidine block as in Fig. 3 and imaged cells every 20 minutes for 24 h following thymidine release to acquire dynamic single-cell pHi measurements. We observed bursts of mitotic cells at 15 h±4 h, indicating thymidine was synchronizing individual cells. Representative stills of ratiometric time-lapse pHi imaging in a dividing cell are shown (Fig. 4A, Video S1). For this cell, pHi

bioRxiv preprint doi: https://doi.org/10.1101/2021.06.04.447151; this version posted June 7, 2022. The copyright holder for this preprint (which was not certified by peer review) is the author/funder, who has granted bioRxiv a license to display the preprint in perpetuity. It is made available under aCC-BY-NC-ND 4.0 International license.

quantification shows increasing pHi through late S and G2 phases (as determined by Fig. 3 cyclin data), acidification just before mitosis, and pHi recovery in daughter cells (Fig. 4B). To investigate and compare trends in single-cell pHi dynamics over the cell cycle, we selected prophase as a "normalization point" for each individual dividing cell. Prophase was chosen because DNA condensation was easily identified using live-cell DNA staining. When pHi dynamics were plotted for 39 dividing cells, we observed a significant period of alkalization that began ~11 h prior to division and persisted until prophase (Fig. 4C). Parent cells that divided within the 24 h period showed a significantly higher median pHi increase (0.16±0.07; Fig. 4D) when compared to nondividing cells (0.10±0.03; Fig. 4D). These data suggest that increased pHi dynamics may be required to signal a cell to divide. Prior work on pHi in migration (Martin et al., 2011b) and cell cycle progression (Flinck et al., 2018a) show pHi increases of 0.2 at the population level are capable of altering these cell behaviors at the population level. These single-cell data suggest that the pHi dynamics measured in dividing single cells are within the reported physiological range for pHi-dependent regulation of cell behaviors.

The single-cell pHi increases measured prior to division in the time-lapse experiments correlate with the increased pHi observed during G2/M in the discontinuous endpoint data (Fig. 2I, 3I, S5E). Interestingly, these single-cell data also reveal a significant acidification event in single cells following prophase, which may correlate with the acidification observed in the discontinuous H1299-mCh-pHl and A549-mCh-pHl cells after mitosis (Fig. 3I, S5E). Although we were able to measure pHi dynamics during G2/M via DNA condensation, we were not able to confidently measure where the S/G2 transition

bioRxiv preprint doi: https://doi.org/10.1101/2021.06.04.447151; this version posted June 7, 2022. The copyright holder for this preprint (which was not certified by peer review) is the author/funder, who has granted bioRxiv a license to display the preprint in perpetuity. It is made available under aCC-BY-NC-ND 4.0 International license.

388 occurred. Therefore, we could not correlate these data with additional pHi changes
389 observed in the endpoint data, including decreased pHi during S phase (Fig. 2I, 8-12h;
390 Fig. 3I, 4 h).
391

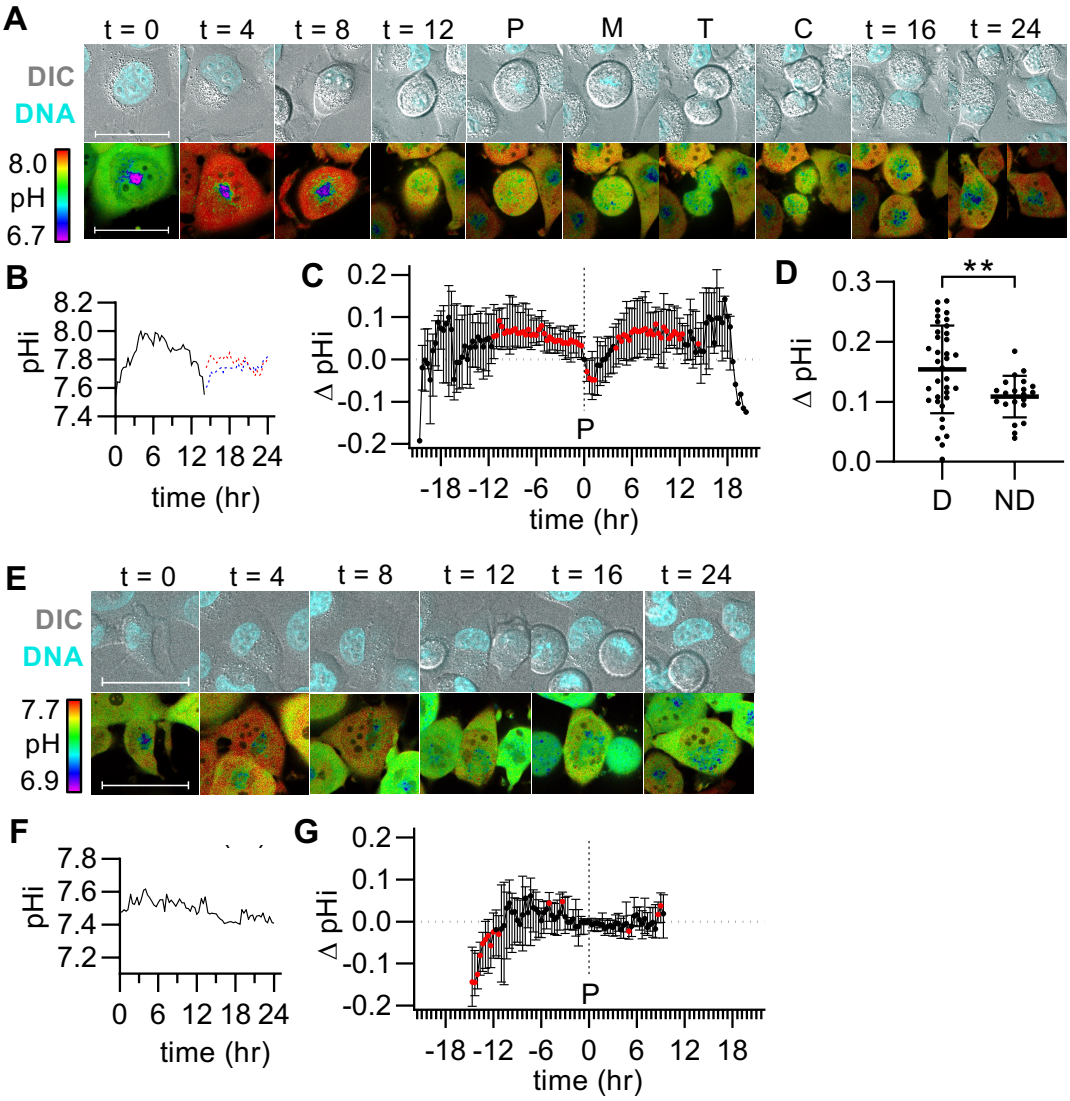


392 **Figure 4: Intracellular pH increases leading to G2/M, followed by rapid acidification**
393 **prior to division and recovery of daughter cells.**
394 A) Representative stills of Video S1 of a dividing H1299-mCh-pHl cell at indicated time
395 (h). Top is Hoescht dye (DNA, cyan) and DIC merge. Bottom is ratiometric display of
396 pHluorin/mCherry fluorescence ratios, scale bars: 50 μm. B) Traces of calculated pHi
397 values of the cell in A) (black, solid line) and in daughter cells (red and blue dotted lines).

bioRxiv preprint doi: https://doi.org/10.1101/2021.06.04.447151; this version posted June 7, 2022. The copyright holder for this preprint (which was not certified by peer review) is the author/funder, who has granted bioRxiv a license to display the preprint in perpetuity. It is made available under aCC-BY-NC-ND 4.0 International license.

C) pHi changes in dividing cells, relative to pHi at prophase (P) for each individual cell (median±IQ range, n=39, 3 biological replicates). Significance determined by a one-sample Wilcoxon test compared to 0 (red points, *p<0.05). D) Scatter plot of max pHi change in individual dividing (D) and non-dividing (ND) cells (mean±SD). Significance determined by an unpaired t-test (**p<0.01). E) Representative stills of Video S2 of a non-dividing H1299-mCh-pHI cell at indicated time (h). Top is Hoescht dye (DNA, cyan) and DIC merge. Bottom is ratiometric display of pHluorin/mCherry fluorescence ratios, scale bars: 50 μm. F) Trace of pHi values of cell in E) (black, solid line) over time. G) pHi changes in non-dividing cells, relative to the pHi at average time of prophase (determined from dividing cell data) (median±IQ range, n=22, from 3 biological replicates). Significance determined by a one-sample Wilcoxon test compared to 0 (red points, *p<0.05).

Although we saw a burst of mitotic cells after thymidine release that validates our synchronization was effective, there was some variability in the timing of prophase (Fig. S7A) and heterogeneity in the magnitude of pHi changes from prophase (Fig. 4D, S7B). To confirm that alkalinization was correlated with cell-cycle timing vs. imaging timing, we binned dividing cells according to prophase time. We observed significant alkalizations in each group pre- and post-prophase, with a significant alkalinization point at ~5 h prior to prophase regardless of timing of prophase (Fig. S7C). Previous data using FUCCI cell cycle reporters found late S/G2 length ranging from ~5-13 h in H1299 cells (Rajal et al., 2021). Additionally in our own data (shown below), we measured 4.3 h as the average G2 length. Taken together, these data suggest that the increase in pHi at 5 h may be occurring at the S/G2 transition. This significant pHi increase is also observed in the time-lapse traces (Fig. 4C) and the single-cell endpoint data corresponding to S/G2 cyclin markers (Fig. 2I, 12 h; Fig. 3I, 4 h). These data suggest that increased pHi may be a permissive cue for G2 phase entry.

The single-cell time-lapse analysis allows us to differentiate between cells that undergo mitosis and cells that do not. If pHi dynamics are a sufficient regulator of cell cycle progression, we may expect to see attenuated pHi dynamics in non-dividing cells. To test

bioRxiv preprint doi: https://doi.org/10.1101/2021.06.04.447151; this version posted June 7, 2022. The copyright holder for this preprint (which was not certified by peer review) is the author/funder, who has granted bioRxiv a license to display the preprint in perpetuity. It is made available under aCC-BY-NC-ND 4.0 International license.

this hypothesis, we quantified pHi from non-dividing cells in our dataset. Representative stills of ratiometric time-lapse pHi imaging in a non-dividing cell are shown in Fig. 4E (Video S2). This non-dividing cell showed attenuated pHi dynamics compared to dividing cells (Fig. 4F). To compare trends in single-cell pHi dynamics for non-dividing cells, delta pHi was calculated for each non-dividing cell from the average prophase timing in dividing cells (15 h) (Fig. 4G). When pHi data from the 22 non-dividing cells were analyzed, we observed attenuated pHi dynamics with the only significant changes coming from a short period of alkalization after release (Fig. 4G). Importantly, the significant alkalization we observe in dividing cells in the ~5 hours prior to prophase (Fig. 4C, Fig. S7C) is not observed in the non-dividers, indicating that single-cell pHi dynamics may be correlated with (or regulate) single-cell cell cycle progression.

S phase is associated with increased protein expression (Aviner et al., 2015). To confirm that the alkalinization we observed in S phase is not an artifact of increased mCh-pHl biosensor expression, we tracked mCherry and pHluorin intensities over time in both dividers and non-dividers (Fig. S8). If the alkalinization is artifactual, we would expect to see increases in the pH-insensitive mCherry fluorescence in dividers specifically, indicating increased protein expression during S phase. Instead, we observe that mCherry fluorescence similarly decreases after initial acquisition (photobleaching) followed by a stabilization in both dividers and non-dividers (Fig. S8A). Furthermore, the pHluorin increases observed over time in dividing cells are not correlated with increased mCherry fluorescence, which indicates pHluorin increases are not due to increases in biosensor expression (Fig. S8B-C).

bioRxiv preprint doi: https://doi.org/10.1101/2021.06.04.447151; this version posted June 7, 2022. The copyright holder for this preprint (which was not certified by peer review) is the author/funder, who has granted bioRxiv a license to display the preprint in perpetuity. It is made available under aCC-BY-NC-ND 4.0 International license.

## Dysregulated pHi dynamics affect cell cycle phase duration and cause phase-specific arrests

We have shown that after synchronization with Palbociclib (Fig. 2) and thymidine (Fig. 3), pHi is dynamic and correlates with cell cycle phases. To compare pHi data from both synchronization techniques, we aligned pHi data (Fig. 2I, Fig 3I) according to significantly increased cyclin B1 expression (Fig. 2H, Fig. 3H) and found oscillating pHi dynamics through the cell cycle (Fig. 5A). We observed that pHi decreases during G1/S, increases in mid-S phase, decreases leading to S/G2, and increases leading to G2/M (Fig. 5A). In addition, our time-lapse data uncovered rapid acidification during M phase leading to division (Fig. 4C). These data suggest a correlation between pHi and cell cycle progression, but to determine a causal relationship, we needed the ability to change pHi and determine effects on cell cycle phases in real-time. To do this, we used established pHi manipulation techniques (White et al., 2017b; Larsen et al., 2012) and the FUCCI cell cycle reporter to track single cells during cell cycle progression using time-lapse microscopy.

FUCCI reporters use regulatory domains of cell-cycle proteins to differentially express fluorescent proteins and report on cell cycle progression in single cells (Fig. 5B). We selected the PIP-FUCCI reporter, which allows improved delineation of S phase (Grant et al., 2018) compared to older FUCCI variants. The PIP-FUCCI reporter fluorescence is driven by regulatory domains PCNA interacting protein degron from human $Cdt1_{1-17}$ (PIP) fused to mVenus and $Geminin_{1-110}$ fused to mCherry. PIP-mVenus accumulates in the

bioRxiv preprint doi: https://doi.org/10.1101/2021.06.04.447151; this version posted June 7, 2022. The copyright holder for this preprint (which was not certified by peer review) is the author/funder, who has granted bioRxiv a license to display the preprint in perpetuity. It is made available under aCC-BY-NC-ND 4.0 International license.

nucleus during G1 and is rapidly lost the during onset of DNA replication (S phase). At the beginning of S phase, mCherry-Geminin accumulates and is expressed throughout S, G2, and M phases. During the S-G2 transition, mVenus accumulates again, and both mVenus and mCherry are co-expressed until division. Thus, the PIP-FUCCI reporter system enables accurate delineation of G1/S and S/G2. M phase is marked by nuclear envelope breakdown and diffusion of mVenus and mCherry signals throughout the cell. Mitosis and cytokinesis can also be monitored by DNA stain and DIC imaging (Fig. 5C). Following cytokinesis, only mVenus is expressed in the two daughter cell nuclei, marking G1. A schematic of cell fluorescence expression and fluorescent intensity traces for mVenus and mCherry throughout the cell cycle are shown in Fig. 5B.

To directly compare pHi and cell cycle, PIP-FUCCI was stably expressed in H1299 cells (H1299-FUCCI) (Fig. 5C, Video S3), and we used pHi manipulation conditions to experimentally lower and raise pHi. A combination of two small molecule inhibitors was used to lower pHi: 5-(N-ethyl-N-isopropyl) amiloride (EIPA), which inhibits NHE1 (White et al., 2017b) and 2-chloro-N-[[2′-[(cyanoamino)sulfonyl][1,1′-biphenyl]-4-yl]methyl]-N-[(4-methylphenyl)methyl]-benzamide (S0859) (Larsen et al., 2012), which inhibits the $Na^+$-$HCO_3^-$ transporter (NBCn1) (Fig. 5D). To raise pHi, low levels of ammonium chloride ($NH_4Cl$) (White et al., 2017b) were used (Fig. 5D). We then used time-lapse confocal microscopy to measure FUCCI reporter expression in cells over a 36 h period with and without pHi manipulation. Single cells were tracked over time and mVenus and mCherry fluorescent intensities were analyzed to determine lengths of single-cell cell cycle phases (see methods for details). Cells that were in G1 phase at the start of treatment with E+S

bioRxiv preprint doi: https://doi.org/10.1101/2021.06.04.447151; this version posted June 7, 2022. The copyright holder for this preprint (which was not certified by peer review) is the author/funder, who has granted bioRxiv a license to display the preprint in perpetuity. It is made available under aCC-BY-NC-ND 4.0 International license.

(low pHi) and $NH_4Cl$ (high pHi) conditions were analyzed for successful completion of a full cycle compared to untreated (control) cells (Fig. 5E). In both conditions, cells successfully completed G1/S, but only 10.2% of low pHi cells successfully entered G2. Subsequently, no low pHi cells starting in G1 phase could reach M phase and divide. Cells in G1 with high pHi were able to complete the cell cycle at rates similar to control cells (Fig 5E). Next, dividing cells in each treatment condition were plotted as single-cell traces of FUCCI fluorescence intensities (mVenus, mCherry) and aligned to division time (Fig. 5F-H). From these traces, we observed overall fewer divisions for low pHi cells (37.5%), and only low pHi cells in G2 or M phase at the start of treatment were able to divide (Fig. 5F). High pHi induced phase elongation in parental cells prior to division, read out by elongated mVenus and mCherry traces compared to control (Fig. 5H). G1 phase (high mVenus, low mCherry) is appreciably shortened in daughter cells at low pHi (Fig. 5F) while high pHi generally elongated G1 (Fig. 5H) compared to control (Fig. 5G).

To investigate this G1 phase shortening/elongation, we quantified all cell cycle phase durations under control, high, and low pHi conditions. Using fluorescence intensity cutoffs to determine G1/S and S/G2 (Fig. 5B, see methods), we measured significant differences in phase durations with high and low pHi conditions (Fig. 5I-J, L). We found that G1 phase in daughter cells was significantly shortened at low pHi (1.7±0.4 h) and significantly elongated at high pHi (8.7±2.3h) compared to control cells (6.3±1.8 h) (Fig. 5I). These pHi-dependent changes in G1 phase duration suggest that low pHi is a permissive cue for G1 exit and that aberrant alkalization can delay this cell-cycle transition. These data align with the measured decrease in pHi at G1/S in endpoint assays (Fig. 5A).

bioRxiv preprint doi: https://doi.org/10.1101/2021.06.04.447151; this version posted June 7, 2022. The copyright holder for this preprint (which was not certified by peer review) is the author/funder, who has granted bioRxiv a license to display the preprint in perpetuity. It is made available under aCC-BY-NC-ND 4.0 International license.

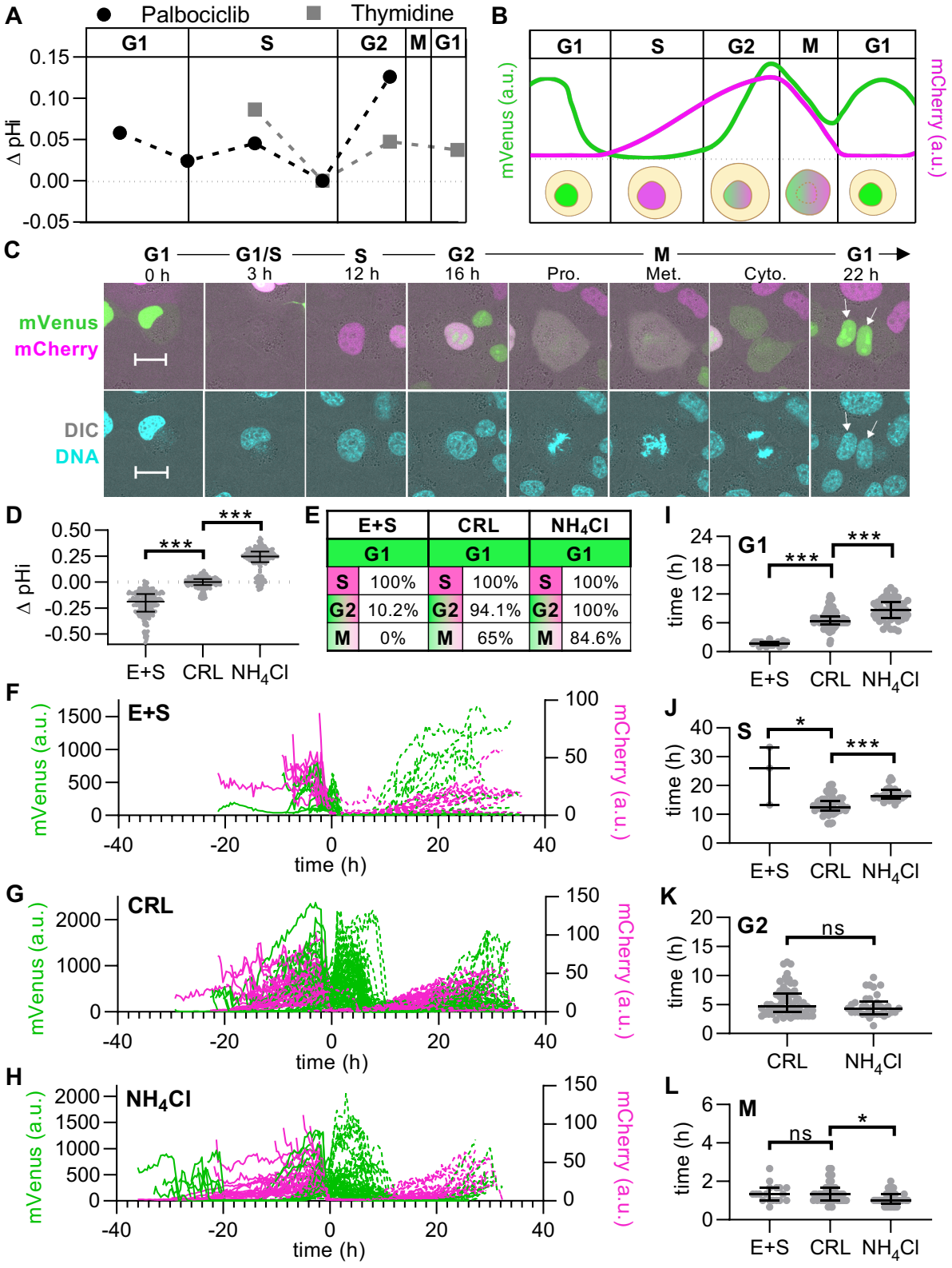


520 **Figure 5: pHi dynamics are key regulators of cell cycle and time G1 exit and S phase**
521 **duration.** A) Median plots of single-cell delta pHi from peak cyclin B1 (thymidine, 4 h;

bioRxiv preprint doi: https://doi.org/10.1101/2021.06.04.447151; this version posted June 7, 2022. The copyright holder for this preprint (which was not certified by peer review) is the author/funder, who has granted bioRxiv a license to display the preprint in perpetuity. It is made available under aCC-BY-NC-ND 4.0 International license.

Palbociclib, 12 h). Data reproduced from Fig. 2I and 3I. (thymidine, n=4; Palbociclib, n=3) B) Schematic of PIP-FUCCI reporter fluorescence traces and cell cycle phases (Grant et al., 2018). C) Representative stills of Video S3. Shown is a single H1299-FUCCI cell with PIP-mVenus (green) and mCherry-Geminin (magenta) tracked through each cell cycle phase. Hoescht dye (DNA, cyan) and DIC merge shown and daughter cells indicated (arrowheads); scale bars: 50 μm. D) Single-cell pHi of H1299-FUCCI cells treated with EIPA and SO859 (E+S, n=233) to lower pHi, untreated (CRL, n=267), or treated with ammonium chloride ($NH_4Cl$, n=202) to raise pHi (see methods for details). E) Progression success of cells in G1 treated as in D. E+S (n=28), CRL (n=17), or $NH_4Cl$ (n=13). F-H) PIP-mVenus (green) and mCherry-Geminin (magenta) fluorescence intensity traces from single H1299-FUCCI cells treated as in D. Traces aligned at time of division at 0 h and daughter cell pHi indicated by dotted lines: F) E+S, (n=23); G) CRL (n=126); H) $NH_4Cl$ (n=72). (CRL and $NH_4Cl$: 3 biological replicates, E+S, 2 biological replicates). I-L) Cell cycle phase durations of cells in F-H. I) G1 (E+S, n=22; CRL, n=100; $NH_4Cl$, n=51) J) S (E+S, n=3; CRL, n=67; $NH_4Cl$, n=26), K) G2 (CRL, n=65; $NH_4Cl$, n=34), and L) M (E+S, n=18; CRL, n=77; $NH_4Cl$, n=33). For D and I-L, scatter plots (median±IQ range), with Mann-Whitney test to determine statistical significance (*p<0.05; ***p<0.001).

After G1 phase completion, we found that high pHi significantly elongated S phase (16.3±2.4 h) compared to control (12.3±3.0 h), while low pHi inhibited the S/G2 transition for all but 10.4% of cells (Fig. 5J). This suggests that high pHi is a requirement for S phase transition to G2, but there is also a need for low pHi for proper timing of S phase duration compared to control cells. The requirement for an increase and decrease in pHi is supported by our synchronized single-cell pHi data, which showed an increase in pHi during mid-S phase and a decrease in late S phase or near the S/G2 transition (Fig. 5A). Our data suggests that without an increase in pHi, cells cannot transition from S to G2 phase, but also that dynamic pHi is required for correct timing of S phase.

During G2 phase, we did not measure a significant difference in phase length with high pHi compared to control (Fig. 5J). Low pHi cells could not complete the S/G2 transition, therefore no G2 phase times could be measured. As previously mentioned, M phase

bioRxiv preprint doi: https://doi.org/10.1101/2021.06.04.447151; this version posted June 7, 2022. The copyright holder for this preprint (which was not certified by peer review) is the author/funder, who has granted bioRxiv a license to display the preprint in perpetuity. It is made available under aCC-BY-NC-ND 4.0 International license.

554 duration for low pHi cells could be measured only for cells in G2 or M during the start of
555 the experiment. We hypothesized that if a high pHi threshold was already met during early
556 G2, low pHi cells had the ability to complete division. This hypothesis aligns with our time-
557 lapse data showing high pHi 5 h prior to division followed by rapid acidification during
558 mitosis (Fig. 4C, S7C).
559 We were surprised to see a significant shortening of M phase with high pHi, as we
560 expected the lack of acidification to elongate M phase. However, previous work in lower-
561 order organisms showed that high pHi stabilizes microtubules (Gagliardi and Shain, 2013;
562 Schatten et al., 1986) and low pHi caused metaphase arrest (Watanabe et al., 1997), so
563 if cells can more rapidly assemble the spindle during early M phase, that could lead to a
564 shorter progression to division. While future work will explore the molecular mechanisms
565 driving the shortening/elongation of cell cycle phases, our results suggest that a decrease
566 in pHi is a cue for G1 exit, increases/decreases are required for S phase, and increases
567 are necessary for G2 entry.
568
569 These single-cell measurements, both via endpoint assays and single-cell time-lapse
570 measurements, show novel pHi dynamics through the cell cycle. Our data support prior
571 work using ion transporter knockdown to show that high pHi regulates S phase length
572 (Flinck et al., 2018b) and G2/M (Putney and Barber, 2003). However, our work also
573 reveals novel decreases in pHi during G1/S, late S, and mitosis (Fig. 6). Our combined
574 use of single-cell pHi manipulation and cell cycle reporters show that pHi plays an
575 important role in regulating the cell cycle, particularly for correct timing of G1 exit, S phase

bioRxiv preprint doi: https://doi.org/10.1101/2021.06.04.447151; this version posted June 7, 2022. The copyright holder for this preprint (which was not certified by peer review) is the author/funder, who has granted bioRxiv a license to display the preprint in perpetuity. It is made available under aCC-BY-NC-ND 4.0 International license.

progression, and G2 entry (Fig. 6. Our work suggests single-cell pHi not only reports on but regulates the essential cell function of cell cycle progression.

## DISCUSSION

Intracellular pHi dynamics have been implicated in diverse cellular processes like differentiation (Ulmschneider et al., 2016), proliferation (Flinck et al., 2018a), migration (Martin et al., 2011a), and apoptosis (Sergeeva et al., 2017). However, we have a limited mechanistic understanding of how spatiotemporal and single-cell pHi dynamics regulate cell behaviors. This is partially due to reliance on population analyses, non-physiological environments, or genetic ion transporter ablation approaches to link pHi and phenotype (Czowski et al., 2020).

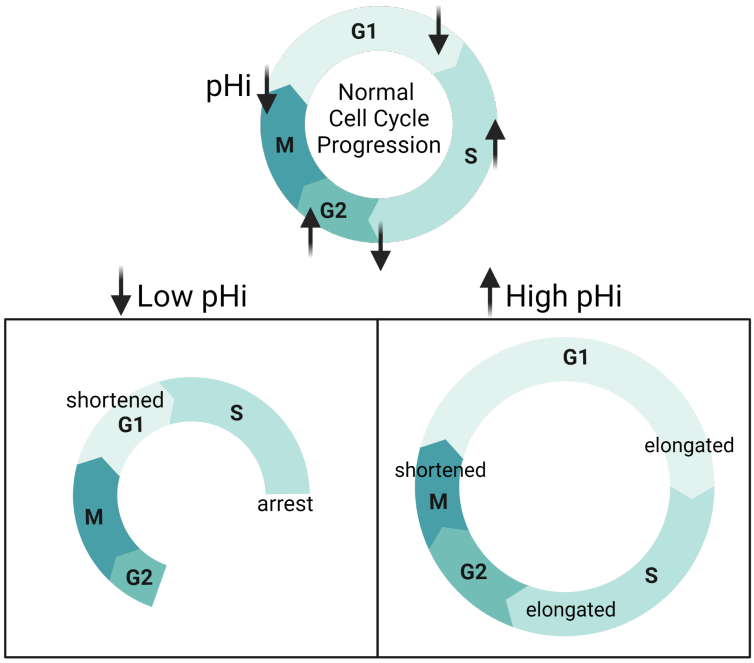


**Figure 6: Single-cell pHi is dynamic during cell cycle progression and regulates G1 exit, S phase duration, and S/G2 transition.** During cell cycle progression, pHi decreases at the G1/S boundary, increases in mid-S phase before dropping in late S, increases through G2 and decreases leading to division. When pHi is experimentally lowered, cells have a shortened G1 and S phase arrests. With high pHi conditions, G1 and S phases

bioRxiv preprint doi: https://doi.org/10.1101/2021.06.04.447151; this version posted June 7, 2022. The copyright holder for this preprint (which was not certified by peer review) is the author/funder, who has granted bioRxiv a license to display the preprint in perpetuity. It is made available under aCC-BY-NC-ND 4.0 International license.

592 are elongated, and M phase is shortened. This suggests that low pHi cues G1 exit and
593 high pH is necessary for G2 entry.
594

595 Here, we present two results linking single-cell pHi and non-genetic phenotype. First, our
596 single-cell pHi measurements confirm that pHi is heterogeneous even in genetically-
597 identical clonal cell lines, suggesting pHi may correlate with non-genetic phenotypic
598 variation. Second, we demonstrate using single-cell approaches that transformed cells
599 have a higher median pHi than normal cells, agreeing with population-level analyses that
600 suggest cancer cells have a constitutively increased pHi homeostasis compared to
601 normal cells (White et al., 2017a). However, our single-cell analyses reveal that pHi
602 heterogeneity is similar when compared across normal and transformed cell lines. This
603 result was surprising, as we hypothesized that pHi heterogeneity might reflect the
604 increased phenotypic heterogeneity in cancer (Hinohara and Polyak, 2019). A future goal
605 is to more closely examine whether pHi is predictive of phenotype (i.e. can pHi be used as a
606 biomarker of more cryptic phenotypic markers of cells such as cell cycle status, metabolic
607 activity, and growth factor signaling heterogeneity). The fact that in our data the average
608 pHi increased with metastatic potential suggests that pHi could be used to identify cancer
609 vs. normal tissue at the single-cell level.
610

611 We also characterized the relationship between pHi and cell cycle progression. Prior work
612 at the population level using genetic ablation of ion transporters and non-native
613 environments suggested a role for pHi in regulating cell cycle progression (Flinck et al.,
614 2018a). We show that single-cell pHi is dynamic over an entire cell cycle, with pHi
615 significantly decreasing at the G1/S boundary, increasing in mid-S before dropping in late
616 S phase, alkalinizing through G2 and peaking at G2/M, and finally acidifying during

bioRxiv preprint doi: https://doi.org/10.1101/2021.06.04.447151; this version posted June 7, 2022. The copyright holder for this preprint (which was not certified by peer review) is the author/funder, who has granted bioRxiv a license to display the preprint in perpetuity. It is made available under aCC-BY-NC-ND 4.0 International license.

617 mitosis followed by pHi recovery in daughter cells. Here, we present three key results
618 suggesting a regulatory link between pHi dynamics and cell cycle at both the population
619 and single-cell levels.
620
621 First, we show for that pHi significantly decreases at the G1/S boundary. These results
622 were consistent across multiple cell lines regardless of which cell cycle synchronization
623 method was used. Our single-cell pHi manipulation data suggest that decreased pHi is a
624 permissive cue for G1 exit. Low pHi significantly shortened G1, while high pHi conditions
625 significantly elongated G1 compared to control. These results indicate a novel regulatory
626 role for pHi acidification in regulating G1 exit.
627
628 Second, we show that pHi increases in mid-S phase and decreases before the S/G2
629 transition. Dynamic pHi, both increases and decreases, are important for proper timing of
630 S phase. Low pHi inhibited the S/G2 transition and while high pHi allowed for S/G2, these
631 cells spent a significantly longer time in S phase compared to control. The single-cell pHi
632 manipulation data suggests that increased pHi is necessary for successful entry into G2.
633 This confirms results at the population level showing pHi increases in S phase (Flinck et
634 al., 2018b) and successful transition through G2/M (Putney and Barber, 2003). But our
635 work also reveals novel decreases in pHi that may be necessary for successfully timed
636 G1/S and S/G2 transitions
637
638 Third, we show that single-cell pHi dynamics peak at G2/M and rapidly acidified during M
639 phase. The increase in pHi during G2/M confirms prior work showing that increased pHi

bioRxiv preprint doi: https://doi.org/10.1101/2021.06.04.447151; this version posted June 7, 2022. The copyright holder for this preprint (which was not certified by peer review) is the author/funder, who has granted bioRxiv a license to display the preprint in perpetuity. It is made available under aCC-BY-NC-ND 4.0 International license.

correlated with increased G2/M transition (Putney and Barber, 2003; Sellier et al., 2006). However, our data also suggest a novel role for intracellular acidification during late M phase and division. Future work using time-lapse imaging and applying optogenetic tools to spatiotemporally change pHi (Donahue et al., 2021) will be required to further characterize M phase pHi dynamics.

Single-cell techniques can elucidate single-cell behaviors and heterogeneity not found at the population level. Here, we addressed a critical need in the field to understand how pHi dynamics regulate single cells during cell cycle progression. These pHi dynamics could be essential for understanding complex cell biology that integrates single-cell and tissue-level behaviors. For example, prior work showed pHi gradients are generated in morphogenetic tissues (Weiß and Bohrmann, 2019). Our work now supports the hypothesis that bursts of synchronized cell proliferation may underlie these observations. More work is necessary to determine how temporal pHi gradients occur during cell cycle phase transitions and whether a threshold of pHi changes is required. With our data establishing a framework of pHi regulation during an entire cell cycle, future work will determine which pH-sensitive proteins may be mediating and correctly timing pH-dependent cell cycle progression. The knowledge gained could aid in identifying new therapeutic routes for limiting proliferation and pHi-dependent behaviors in cancer progression.

bioRxiv preprint doi: https://doi.org/10.1101/2021.06.04.447151; this version posted June 7, 2022. The copyright holder for this preprint (which was not certified by peer review) is the author/funder, who has granted bioRxiv a license to display the preprint in perpetuity. It is made available under aCC-BY-NC-ND 4.0 International license.

## MATERIALS AND METHODS

### Cell Culture and Conditions

Complete media for H1299 cells (ATCC CRL-5803): RPMI 1640 (Corning, 10-040-CV) supplemented with 10% Fetal Bovine Serum (FBS, Peak Serum, PS-FB2); A549 (ATCC CCL-185): DMEM (Corning, MT10013CVV) supplemented with 10% FBS; and NL20 (ATCC CRL-2503): Ham's F12 (Lonza, 12001-578) supplemented with 4% FBS, 1.5 g/L sodium bicarbonate (Sigma, S6014), 2.7 g/L glucose (VWR, BDH9230), 2.0 mM Glutamax (Gibco, 35050079), 0.1 mM nonessential amino acids (Lonza, BW13114E), 0.005 mg/mL insulin (Sigma, I1882), 10 ng/mL EGF (Peprotech, AF-100-15), 0.001 mg/mL transferrin (BioVision, 10835-642), 0.0005 mg/mL hydrocortisone (Sigma, H0888). All cells were maintained at 5% $CO_2$ and 37°C in a humidified incubator.

### Transfections and stable cell line selection

H1299 cells were transfected with the pCDNA3-mCherry-SEpHluorin (Koivusalo et al., 2010) (mCh-pHl) or pLenti-CMV-Blast-PIP-FUCCI using Lipofectamine2000 (Life Technologies, 11668019) per manufacturer's instructions. After 24 h, cells were trypsinized and plated at low dilution in a 10 cm dish with media containing 0.8 mg/mL Geneticin. Cloning cylinders were used to select colonies expressing mCh-pHl for expansion. A final clone was selected based on microscopy assay for mCh-pHl expression and comparison of cell morphology and pHi to parental H1299. For H1299-FUCCI, cells were trypsinized after 24 h transfection and plated at low dilutions (50 cells/mL) in a 96 well plate in media containing 0.5 mg/mL Blasticidin. Wells with equal

bioRxiv preprint doi: https://doi.org/10.1101/2021.06.04.447151; this version posted June 7, 2022. The copyright holder for this preprint (which was not certified by peer review) is the author/funder, who has granted bioRxiv a license to display the preprint in perpetuity. It is made available under aCC-BY-NC-ND 4.0 International license.

684 expression were further expanded and screened on a microscopy assay for FUCCI
685 expression and for similar cell morphology and pHi compared to parental H1299.
686
687 Lentiviral transfection was used to generate stable mCh-pHl expression in NL20 and
688 A549 cells. Production of the virus was carried out in 293FT cells. Cells were grown to
689 near confluency in a 10 cm dish and transfected with plx304-mCherry-SEpHluorin (Gift of
690 Yi Liu and Diane Barber at UCSF) and two packaging plasmids: PSPAX2 (Addgene
691 #12260) and PMD2.6 (Addgene #12259) provided by Siyuan Zhang (University of Notre
692 Dame). Three µg each of the plx304-mCherry-pHluorin, PSPAX2, and PDM2.6 were
693 transfected into a nearly confluent 10 cm dish of 293FT cells using Lipofectamine2000
694 for 18 h. Media was changed and incubated another three days. Viral supernatant was
695 collected from the cells and centrifuged for 15 min at 3000 rpm. The supernatant was
696 passed through a 0.2 µm polyethersulfone filter, flash-frozen in liquid nitrogen in 1 mL
697 aliquots, and stored at -80°C.
698
699 NL20 and A549 cells were plated in a 6-well plate for viral transduction. After 24 h, viral
700 supernatant was diluted 1:1.6, 1:3, and 1:10 into antibiotic-free media (depending on cell
701 line) with 10 µg/mL Polybrene (Sigma, TR-1003-G), added to separate wells and
702 incubated for 48-72 hr. Transduced cells were moved to a 10 cm dish and selected with
703 0.5 mg/mL Blasticidin (Fisher, BP264725). NL20 cells were plated at low density in 96
704 well plates (0.5 cells/well). Colonies expressing mCh-pHl were expanded, and a final
705 NL20-mCh-pHl clone was chosen based on microscopy assay for mCh-pHl expression
706 and comparison to morphology and pHi of parentals. A549 cells were sorted using

bioRxiv preprint doi: https://doi.org/10.1101/2021.06.04.447151; this version posted June 7, 2022. The copyright holder for this preprint (which was not certified by peer review) is the author/funder, who has granted bioRxiv a license to display the preprint in perpetuity. It is made available under aCC-BY-NC-ND 4.0 International license.

fluorescence-activated cell sorting (FACS), and a population sort according to mCherry expression was used for all imaging experiments after confirmation with microscopy.

**BCECF plate reader assays**

Cells were plated at $4.0x10^5$ - $8.0x10^5$ cells/well in a 24-well plate and incubated overnight. Cells were treated with 2 μM 2',7'-Bis-(2-Carboxyethyl)-5-(and-6)-Carboxyfluorescein, Acetoxymethyl Ester (BCECF-AM) (VWR, 89139-244) for 30 min at 37°C and 5% $CO_2$. NL20 and H1299 cells were washed 3x5 minutes with a pre-warmed (37°C) HEPES-based wash buffer (30 mM HEPES pH 7.4, 145 mM NaCl, 5 mM KCl, 10 mM glucose, 1 mM $MgSO_4$, 1 mM $KHPO_4$, 2 mM $CaCl_2$, pH 7.4) and A549 cells were washed 3x5 minutes with a pre-warmed (37°C) Bicarbonate ($HCO_3$)-based wash buffer (25 mM $HCO_3$, 115 mM NaCl, 5 mM KCl, 10 mM glucose, 1 mM $MgSO_4$, 1 mM $KHPO_4$, 2 mM $CaCl_2$, pH 7.4). Two Nigericin buffers (25 mM HEPES, 105 mM KCl, 1 mM $MgCl_2$) were supplemented with 10 μM nigericin (Fisher, N1495), pH was adjusted to ~6.7 and ~7.7, and were pre-warmed to 37°C. Fluorescence was read (ex 440, em 535; ex 490, em 535) on a Cytation 5 plate reader incubated at 37°C with 5% $CO_2$. Kinetic reads were taken at 15-sec intervals for 5 min, using a protocol established within Gen5 software. After the initial pHi read, the HEPES/bicarbonate wash was aspirated and replaced with one of the nigericin buffer standards, and cells were incubated at 37°C with 5% $CO_2$ for 7 min. BCECF fluorescence was read by plate reader as above. This process was repeated with the second nigericin standard. The mean intensity ratio (490/440) was derived from each read. Measurements were calculated from a nigericin linear regression using exact nigericin buffer pH to the hundredths place (Grillo-Hill et al., 2014).

bioRxiv preprint doi: https://doi.org/10.1101/2021.06.04.447151; this version posted June 7, 2022. The copyright holder for this preprint (which was not certified by peer review) is the author/funder, who has granted bioRxiv a license to display the preprint in perpetuity. It is made available under aCC-BY-NC-ND 4.0 International license.

730

731 **Microscopy**

732 Imaging protocol was derived from Grillo-Hill et al. Cells were plated on a 35 mm imaging
733 dish with a 14 mm glass coverslip (Matsunami, D35-14-1.5-U) a day before imaging.
734 Microscope objectives were preheated to 37°C, and the stage-top incubator was
735 preheated to 37°C and kept at 5% $CO_2$/95% air. Confocal images were collected on a
736 Nikon Ti-2 spinning disk confocal with a 40x (CFI PLAN FLUOR NA1.3) oil immersion
737 objective. The microscope is equipped with a stage-top incubator (Tokai Hit), a Yokogawa
738 spinning disk confocal head (CSU-X1), four laser lines (405nm, 488nm, 561 nm, 647 nm),
739 a Ti2-S-SE motorized stage, multi-point perfect focus system, and an Orca Flash 4.0
740 CMOS camera. Hoescht dye (405 laser ex, 455/50 em), pHluorin (488 laser ex, 525/36
741 em), TxRed (561 laser ex, 605/52 em), and mCherry (561 laser ex, 630/75 em) were
742 used. Acquisition times for each fluorescence acquisition ranged from 100-800
743 milliseconds.
744 For imaging, initial fields of view (FOV) were collected on the cells in their respective
745 media. For all imaging, nigericin buffers were prepared identically to BCECF assays, and
746 all buffer exchanges were carried out on the stage incubator to preserve XY positioning.
747 Multiple Z-planes were collected with the center focal plane maintained using a Perfect
748 Focus System (PFS).

749

750 **Single-cell pHi measurements**

751 After acquisition, NIS Analysis Software was used to quantify pHi. Images were
752 background-subtracted using an ROI drawn on a glass coverslip (determined by DIC).

bioRxiv preprint doi: https://doi.org/10.1101/2021.06.04.447151; this version posted June 7, 2022. The copyright holder for this preprint (which was not certified by peer review) is the author/funder, who has granted bioRxiv a license to display the preprint in perpetuity. It is made available under aCC-BY-NC-ND 4.0 International license.

Individual Regions of Interest (ROI) are drawn for each cell in each condition (initial, high pH nigericin, and low pH nigericin), and mCherry aggregates are removed using thresholding holes. Mean pHluorin and mCherry pixel intensities were quantified for each cell, and pHluorin/mCherry ratios were calculated in excel. A cutoff of 100 a.u. units were used for both pHluorin and mCherry intensity values after exporting. For each cell, nigericin values were used to generate a standard curve, and pHi was back-calculated from the single-cell standard curve.

**Double-Thymidine block**

Cells were plated at 10% confluency in 5 replicate 35 mm glass-bottomed dishes and 5 replicate 6-well plates (for protein lysate collection) and incubated overnight. Dishes were identically treated with 2 mM thymidine (Sigma, T9250) for 18 h, washed with PBS, and incubated with fresh complete media for 9 h, then treated for another 18 h with 2 mM thymidine. Cells were released with a PBS wash and fresh complete media. Imaging of the 0 h time point was initiated 20 min after release. Subsequent imaging was collected at 4, 8, 12, and 24 h after release in respective media. Matched dishes at each time point were washed twice with PBS and frozen at -80°C for protein lysate collection and immunoblot analysis of cyclins.

For time-lapse imaging, the double-thymidine block was used as explained above on a single 35 mm glass-bottomed dish supplemented with 1% Pen/Strep (Corning, 30-001-C1) to avoid bacterial contamination during long-term acquisition. Hoechst 33342 solution (ThermoFisher, 62249) was added to the cells (1:20,000) before release and incubated

bioRxiv preprint doi: https://doi.org/10.1101/2021.06.04.447151; this version posted June 7, 2022. The copyright holder for this preprint (which was not certified by peer review) is the author/funder, who has granted bioRxiv a license to display the preprint in perpetuity. It is made available under aCC-BY-NC-ND 4.0 International license.

for 15 min. Dye and thymidine were removed, and cells were washed with PBS to release cells. Fresh media was added, and images were collected every 20 min for 24 hr. Optimal acquisition parameters were as follows: 700 ms exposure time and 8% laser power for GFP; 700 ms exposure time and 10% laser power for TxRed; and 100 ms exposure time and 5% laser power DAPI. A single Z-plane was collected to avoid photobleaching. Nigericin standards were carried out as previously described (Grillo-Hill et al., 2014).

**Palbociclib Synchronization**

Cells were plated at 10% confluency in 5 replicate 35 mm glass-bottomed dishes and 5 replicate 6-well plates (for protein lysate collection) and incubated overnight. Dishes were identically treated with 0.1 μM Palbociclib (PD-0332991) (Selleck, S1116) for 24 h. Cells were washed with PBS and released with complete fresh media. Imaging of the 0 h time point was initiated 20 min after release. Subsequent imaging was collected at 4, 8, 12, 24, and 36 h post-release in respective media (1 replicate 0-24 h, 2 replicates 0-36 h). Matched dishes at each time point were washed twice with PBS and frozen at -80°C for protein lysate collection and immunoblot analysis of cyclins.

**FUCCI cell cycle assays**

For H1299-FUCCI time-lapses, cells were plated in a 4 well imaging dish (10,000 cells/well) and supplemented with 1% Pen/Strep (Corning, 30-001-C1) to avoid bacterial contamination during long-term acquisition. Hoechst dye was added to the cells (1:20,000) 6-8 h prior to imaging and incubated for 15 min, dye solution was removed, and fresh media was added to the cells. Cells were imaged just prior to pHi manipulation,

bioRxiv preprint doi: https://doi.org/10.1101/2021.06.04.447151; this version posted June 7, 2022. The copyright holder for this preprint (which was not certified by peer review) is the author/funder, who has granted bioRxiv a license to display the preprint in perpetuity. It is made available under aCC-BY-NC-ND 4.0 International license.

then treatments were added to the cultured media and images were collected every 20 min for 36 hr. Optimal acquisition parameters were as follows: 200 ms exposure time and 8% laser power for mVenus; 800 ms exposure time and 10% laser power for mCherry; and 200 ms exposure time and 5% laser power DAPI. A single Z-plane was collected to avoid excess light. Additional water was added to the stage top incubator at 18 h.

After acquisition, NIS Analysis Software was used to quantify individual cell cycle phases. Images were background-subtracted using an ROI drawn on a glass coverslip (determined by DIC). Cells were tracked using NIS Analysis software and nuclear regions of interest (ROI) based on DNA stain. In case of improper tracking, manual tracking was used to redraw ROIs. Manual tracking was also used during mitosis when the signals diffused throughout the cell. mVenus and mCherry intensities were exported from matched single-cell nuclear ROI at each time point over 36 h.

Cell cycle phases were determined by mVenus or mCherry fluorescence intensity. For each individual cell trace, including subsequent daughter cells, an excel macro was used to determine timepoints for mVenus and mCherry cutoffs. G1/S was defined as a decrease in mVenus signal below 5% of maximum mVenus intensity. As validation of G1/S, S phase entry was defined as the first time point after mCherry minimum that showed a 3% (determined from mCherry maximum) increase in mCherry intensity compared to the previous point. S/G2 was defined as point at which mVenus intensity

bioRxiv preprint doi: https://doi.org/10.1101/2021.06.04.447151; this version posted June 7, 2022. The copyright holder for this preprint (which was not certified by peer review) is the author/funder, who has granted bioRxiv a license to display the preprint in perpetuity. It is made available under aCC-BY-NC-ND 4.0 International license.

821 rose above 2% of mVenus maximum. G2/M and M/G1 were defined by nuclear envelope
822 breakdown and division into two daughter cells, respectively.
823
824 For pHi manipulation validation, cells were plated at 20% confluency on a 35 mm imaging
825 dish with a 14 mm glass coverslip and incubated overnight. Cells were treated with a
826 combination of 15 μM EIPA/30 μM SO859 (E+S) or 20 mM $NH_4Cl$ ($NH_4Cl$) diluted in fresh
827 media and incubated for 24 h. Both imaging collection and pHi calculations were
828 completed identically to other single-cell pHi measurement experiments. Treated cells
829 were corrected for photobleaching by collecting images of cells in nigericin buffers (pH
830 7.4) with treatment supplemented but without nigericin present.
831
832 **Western Blot**
833 Protein lysates were collected from 35-mm dishes or 6-well plates frozen at time points
834 matched to imaging. Ice-cold lysis buffer [50 mM TRIS, 150 mM NaCl, 1 mM dithiothreitol
835 (DTT), 1 mM Ethylenediaminetetraacetic acid (EDTA), 1% Triton X-100, Roche Protease
836 Inhibitor Cocktail] was added to the samples and incubated for 15 min on ice. Cells were
837 scraped and centrifuged for 10 min at 13,000 g at 4°C. The supernatant was retained,
838 and protein concentration was determined by Pierce™ BCA (ThermoFisher, 23225)
839 protein assay.
840
841 15 μg protein was loaded onto an SDS-Polyacrylamide gel electrophoresis (PAGE) that
842 was run for 3 h at 120 V in 1X Tris-glycine (3.02 g/L Tris, 14.4 g/L glycine, 1.0 g/L SDS).
843 Either a wet-transfer system or a Trans-Blot Turbo Transfer System (Bio-Rad) was used

bioRxiv preprint doi: https://doi.org/10.1101/2021.06.04.447151; this version posted June 7, 2022. The copyright holder for this preprint (which was not certified by peer review) is the author/funder, who has granted bioRxiv a license to display the preprint in perpetuity. It is made available under aCC-BY-NC-ND 4.0 International license.

844 to transfer the proteins to a polyvinylidene fluoride (PDVF) membrane (pre-wet with
845 methanol). For the wet transfer, 1X transfer buffer (141 g/L Glycine, 0.3 g/L Tris base)
846 with 20% Methanol for 1.5 h at 100 V. For the Trans-Blot Turbo Transfer, Bio-Rad transfer
847 buffer was used according to the manufacturer's protocol (7 min). Membranes were
848 blocked in 5% BSA in TBST (2.42 g/L Tris, 8 g/L NaCl, 0.1% Tween) for 2 h then divided
849 for blotting. Primary antibodies: α-cyclin A2 (1:500; Abcam, ab38), α-cyclin B1 (1:1,000;
850 Cell Signaling, 12231), α-cyclin E1 (1:1000; Cell Signaling, 4129), actin (1:1,000; Santa
851 Cruz, 2Q1055). Membranes were incubated with primary antibody solution overnight at
852 4°C with shaking (4 h at RT with shaking for actin). Membranes were washed 3x10 min
853 TBST at RT with shaking and incubated with secondary antibodies [1:10,000; goat α-
854 mouse IgG HRP (Bio-Rad, 1721011) or goat α-rabbit IgG HRP (Bio-Rad, 1706515)] for 2
855 h at RT with shaking. Membranes were washed 3x10 min TBST at RT with shaking,
856 developed using SuperSignal™ West Pico PLUS Chemiluminescent Substrate
857 (ThermoFisher, 34578), and visualized using a ChemiDoc MP Imaging System (BioRad).
858 ImageJ was used for protein quantification, normalized to loading control.
859
860 **Quantification and Statistics**
861 GraphPad Prism was used to prepare graphs and perform statistical analyses. Normality
862 tests were performed on all data sets and an outlier test using the ROUT method (Q=1%).
863 An unpaired t-test (Fig. S1, Fig. 4D) or paired t-test (Fig. 2F-H; Fig. 3F-H) was used for
864 normal data. A Mann Whitney test was used for non-normal, unpaired data (Fig. 1F-G,
865 Fig. S1, Fig. S3C, Fig. S4C, Fig. S6C, Fig, 5D, 5I-L). For time-lapse data (Fig. 4C, Fig.
866 4G, Fig. S7C), a one-sample Wilcoxon test was used, compared to a theoretical mean of

bioRxiv preprint doi: https://doi.org/10.1101/2021.06.04.447151; this version posted June 7, 2022. The copyright holder for this preprint (which was not certified by peer review) is the author/funder, who has granted bioRxiv a license to display the preprint in perpetuity. It is made available under aCC-BY-NC-ND 4.0 International license.

867 0. For non-normal, unpaired data with more than two sets, a Kruskal-Wallis test with
868 Dunn's multiple comparisons test was used (Fig. 2D and 2I, Fig. S3A, Fig. 3D, Fig. 3I,
869 Fig. S5C, Fig. S5E, Fig. S6A). Values were binned at 0.02 in all frequency distributions.
870 All significance was indicated in figures by the following: *p<0.05; **p<0.01; ***p<0.001.
871

872 **Online supplemental material**

873 Fig. S1 shows that the stable mCh-pHl biosensor expression does not alter pHi
874 compared to parental cell lines. Fig. S2 shows nigericin standardization and
875 pHluorin/mCherry ratios form a standard line to calculate pHi reliably. Fig. S3 shows
876 additional H1299-mCh-pHl Palbociclib synchronization replicates of Fig. 2. Fig. S4
877 shows additional H1299-mCh-pHl thymidine synchronization replicates of Fig. 3. Fig. S5
878 shows that pHi is dynamic after release from G1/S in A549-mCh-pHl cells and
879 correlates with cyclin levels. Fig S6 shows additional A549-mCh-pHl thymidine
880 synchronization replicates of Fig. S5. Fig. S7 illustrates heterogeneous timing of
881 prophase but preserved pHi changes from time-lapse experiments shown in Fig. 3. Fig.
882 S8 shows maturation rates of pHluorin and mCherry and no differences in fluorescent
883 protein synthesis between dividing and nondividing cells. Video 1 was used to produce
884 from Fig. 4A and 4B and demonstrates that the pHi of a dividing cell is dynamic
885 following release from G1/S. Video 2 was used to produce Fig. 4E and 4F and shows
886 that pHi dynamics of a nondividing cell are attenuated following release from G1/S.
887 Video 3 was used to produce Fig. 5C and shows an H1299-FUCCI cell differentially
888 expressing mVenus and mCherry depending on cell cycle phase.
889

890 **Video 1: Single, dividing cell shows dynamic pHi changes during cell cycle**
891 **progression.** Video of a dividing cell over 24 h (20 min intervals). Ratiometric display of
892 pHluorin/mCherry fluorescence ratios. Stills from this video were used to produce Fig. 4A, and
893 ratiometric scale is identical. Annotations show cell of interest and timing of
894 prophase/cytokinesis. Arrows reappear to show two daughter cells, scale bars: 20 μm.

895 **Video 2: Single, non-dividing cell shows attenuated pHi changes during over a 24-hour**
896 **period.** Video of a non-dividing cell over 24 h (20 min intervals). Ratiometric display of
897 pHluorin/mCherry fluorescence ratios. Stills from this video were used to produce Fig. 4E, and
898 ratiometric scale is identical. Annotations show cell of interest at the beginning and end of video,
899 scale bars: 20 μm.

900 **Video 3: PIP-FUCCI accurately reports cell cycle phases using mVenus and mCherry**
901 **expression in H1299 cells.** Video of a dividing H1299-FUCCI cell over 24 h (20 min intervals).
902 Fluorescent imaging of FUCCI reporters (PIP-mVenus, green) and (mCherry-Geminin$_{1\text{-}110}$,
903 magenta) that are differentially expressed through cell cycle. Labels appear as the cell transitions
904 to each phase (G1, S, G2, M, G1), scale bar: 20 μm. Stills from this video were used to produce
905 Fig. 5C.

906

bioRxiv preprint doi: https://doi.org/10.1101/2021.06.04.447151; this version posted June 7, 2022. The copyright holder for this preprint (which was not certified by peer review) is the author/funder, who has granted bioRxiv a license to display the preprint in perpetuity. It is made available under aCC-BY-NC-ND 4.0 International license.

## ACKNOWLEDGEMENTS

We would like to thank Dr. Siyuan Zhang (University of Notre Dame) and Dr. Diane Barber (University of California San Francisco) for plasmids. We would also like to thank members of the White lab for their helpful feedback on the manuscript. Figure schematics created with BioRender.com.

## COMPETING INTERESTS

The authors declare no competing financial or non-financial interests.

## FUNDING

This work was supported by a DP2 (1DP2CA260416-01) to K.A.W.

## AUTHOR CONTRIBUTIONS

JSS & KAW Conception and design. JSS acquisition of data. JSS & KAW analysis and interpretation of data, drafting and revising the article.

## REFERENCES

Aerts, R.J., A.J. Durston, and W.H. Moolenaar. 1985. Cytoplasmic pH and the regulation of the dictyostelium cell cycle. *Cell*. 43:653–657. doi:10.1016/0092-8674(85)90237-5.

Barth, D., and M. Fronius. 2019. Shear force modulates the activity of acid-sensing ion channels at low pH or in the presence of non-proton ligands. *Sci. Rep.* 9.

bioRxiv preprint doi: https://doi.org/10.1101/2021.06.04.447151; this version posted June 7, 2022. The copyright holder for this preprint (which was not certified by peer review) is the author/funder, who has granted bioRxiv a license to display the preprint in perpetuity. It is made available under aCC-BY-NC-ND 4.0 International license.

930 doi:10.1038/s41598-019-43097-7.

931 Bjursell, G., and P. Reichard. 1973. Effects of thymidine on deoxyribonucleoside
932 triphosphate pools and deoxyribonucleic acid synthesis in Chinese hamster ovary
933 cells. *J. Biol. Chem.* 248:3904–3909. doi:https://doi.org/10.1016/S0021-
934 9258(19)43819-2.

935 De Boer, L., V. Oakes, H. Beamish, N. Giles, F. Stevens, M. Somodevilla-Torres, C.
936 DeSouza, and B. Gabrielli. 2008. Cyclin A/cdk2 coordinates centrosomal and
937 nuclear mitotic events. *Oncogene*. 27:4261–4268. doi:10.1038/onc.2008.74.

938 Bolderson, E., J. Scorah, T. Helleday, C. Smythe, and M. Meuth. 2004. ATM is required
939 for the cellular response to thymidine induced replication fork stress. *Hum. Mol.*
940 *Genet.* 13:2937–2945. doi:10.1093/hmg/ddh316.

941 Boron, W.F. 2004. Regulation of intracellular pH. *Am. J. Physiol. - Adv. Physiol. Educ.*
942 28:160–179. doi:10.1152/advan.00045.2004.

943 Bryne Ulmschneider, Bree K. Grillo-Hill, Marimar Benitez, Dinara R. Azimova, D.L.B.
944 and T.G.N. 2016. Increased intracellular pH is necessary for adult epithelial and
945 embryonic stem cell differentiation. *J. Cell Biol.* 215:345–355.
946 doi:10.1083/jcb.201606042.

947 Cardone, R.A., V. Casavola, and S.J. Reshkin. 2005. The role of disturbed pH dynamics
948 and the NA+/H+ exchanger in metastasis. *Nat. Rev. Cancer*. 5:786–795.
949 doi:10.1038/nrc1713.

950 Chang, D.C., N. Xu, and K.Q. Luo. 2003. Degradation of cyclin B is required for the
951 onset of anaphase in mammalian cells. *J. Biol. Chem.* 278:37865–37873.
952 doi:10.1074/jbc.M306376200.

bioRxiv preprint doi: https://doi.org/10.1101/2021.06.04.447151; this version posted June 7, 2022. The copyright holder for this preprint (which was not certified by peer review) is the author/funder, who has granted bioRxiv a license to display the preprint in perpetuity. It is made available under aCC-BY-NC-ND 4.0 International license.

953 Chen, G., and X. Deng. 2018. Cell Synchronization by Double Thymidine Block. *Bio-*
954 *Protocol*. 8. doi:10.21769/bioprotoc.2994.
955 Choi, C.H., B.A. Webb, M.S. Chimenti, M.P. Jacobson, and D.L. Barber. 2013. pH
956 sensing by FAK-His58 regulates focal adhesion remodeling. *J. Cell Biol.* 202:849–
957 859. doi:10.1083/jcb.201302131.
958 Czowski, B.J., R. Romero-Moreno, K.J. Trull, and K.A. White. 2020. Cancer and pH
959 dynamics: Transcriptional regulation, proteostasis, and the need for new molecular
960 tools. *Cancers (Basel).* 12:1–19. doi:10.3390/cancers12102760.
961 Deutsch, C., J.S. Taylor, and D.F. Wilson. 1982. Regulation of intracellular pH by
962 human peripheral blood lymphocytes as measured by 19F NMR. *Proc. Natl. Acad.*
963 *Sci. U. S. A.* 79:7944–7948. doi:10.1073/pnas.79.24.7944.
964 Donahue, C.E.T., M.D. Siroky, and K.A. White. 2021. An Optogenetic Tool to Raise
965 Intracellular pH in Single Cells and Drive Localized Membrane Dynamics. *J. Am.*
966 *Chem. Soc.* 143:18877–18887. doi:10.1021/jacs.1c02156.
967 Flinck, M., S.H. Kramer, and S.F. Pedersen. 2018a. Roles of pH in control of cell
968 proliferation. *Acta Physiol.* 223:e13068. doi:10.1111/apha.13068.
969 Flinck, M., S.H. Kramer, J. Schnipper, A.P. Andersen, and S.F. Pedersen. 2018b. The
970 acid-base transport proteins NHE1 and NBCn1 regulate cell cycle progression in
971 human breast cancer cells. *Cell Cycle*. 17:1056–1067.
972 doi:10.1080/15384101.2018.1464850.
973 Fuster, D., O.W. Moe, and D.W. Hilgemann. 2004. Lipid- and mechanosensitivities of
974 sodium/hydrogen exchangers analyzed by electrical methods. *Proc. Natl. Acad.*
975 *Sci. U. S. A.* 101:10482–10487. doi:10.1073/pnas.0403930101.

bioRxiv preprint doi: https://doi.org/10.1101/2021.06.04.447151; this version posted June 7, 2022. The copyright holder for this preprint (which was not certified by peer review) is the author/funder, who has granted bioRxiv a license to display the preprint in perpetuity. It is made available under aCC-BY-NC-ND 4.0 International license.

976 Gagliardi, L.J., and D.H. Shain. 2013. Is intracellular pH a clock for mitosis? *Theor. Biol.*
977 *Med. Model.* 10. doi:10.1186/1742-4682-10-8.
978 Gillies, R.J., and D.W. Deamer. 1979. Intracellular pH changes during the cell cycle in
979 Tetrahymena. *J. Cell. Physiol.* 100:23–31. doi:10.1002/jcp.1041000103.
980 Grant, G.D., K.M. Kedziora, J.C. Limas, J. Gowen Cook, and J.E. Purvis. 2018.
981 Accurate delineation of cell cycle phase transitions in living cells with PIP-FUCCI.
982 doi:10.1080/15384101.2018.1547001.
983 Grillo-Hill, B.K., C. Choi, M. Jimenez-Vidal, and D.L. Barber. 2015. Increased H+ efflux
984 is sufficient to induce dysplasia and necessary for viability with oncogene
985 expression. *Elife*. 2015:1–31. doi:10.7554/eLife.03270.
986 Grillo-Hill, B.K., B.A. Webb, and D.L. Barber. 2014. Ratiometric Imaging of pH Probes.
987 *In* Methods in Cell Biology. 429–448.
988 Harguindey, S., D. Stanciu, J. Devesa, K. Alfarouk, R.A. Cardone, J.D. Polo Orozco, P.
989 Devesa, C. Rauch, G. Orive, E. Anitua, S. Roger, and S.J. Reshkin. 2017. Cellular
990 acidification as a new approach to cancer treatment and to the understanding and
991 therapeutics of neurodegenerative diseases. *Semin. Cancer Biol.* 43:157–179.
992 doi:10.1016/J.SEMCANCER.2017.02.003.
993 Hinohara, K., and K. Polyak. 2019. Intratumoral heterogeneity: more than just
994 mutations. *Trends Cell Biol.* 29:569–579. doi:10.1016/j.tcb.2019.03.003.
995 Karagiannis, J., and P.G. Young. 2001. Intracellular pH homeostasis during cell-cycle
996 progression and growth state transition in Schizosaccharomyces pombe. *J. Cell*
997 *Sci.* 2929–2941. doi:https://doi.org/10.1242/jcs.114.16.2929.
998 Korenchan, D.E., and R.R. Flavell. 2019. Spatiotemporal pH heterogeneity as a

bioRxiv preprint doi: https://doi.org/10.1101/2021.06.04.447151; this version posted June 7, 2022. The copyright holder for this preprint (which was not certified by peer review) is the author/funder, who has granted bioRxiv a license to display the preprint in perpetuity. It is made available under aCC-BY-NC-ND 4.0 International license.

promoter of cancer progression and therapeutic resistance. *Cancers (Basel).* 11:1026. doi:10.3390/cancers11071026.

Larsen, A.M., N. Krogsgaard-Larsen, G. Lauritzen, C.W. Olesen, S. Honoréhansen, E. Boedtkjer, S.F. Pedersen, and L. Bunch. 2012. Gram-Scale Solution-Phase Synthesis of Selective Sodium Bicarbonate Co-transport Inhibitor S0859: in vitro Efficacy Studies in Breast Cancer Cells. *ChemMedChem*. 7:1808–1814. doi:10.1002/CMDC.201200335.

Lee, A.H., and I.F. Tannock. 1998. Heterogeneity of intracellular pH and of mechanisms that regulate intracellular pH in populations of cultured cells. *Cancer Res.* 58:1901–1908.

Liu, M., H. Liu, and J. Chen. 2018. Mechanisms of the CDK4/6 inhibitor palbociclib (PD 0332991) and its future application in cancer treatment (Review). *Oncol. Rep.* 39:901–911. doi:10.3892/or.2018.6221.

Lobo, R.C., N.E. Hubbard, P. Damonte, H. Mori, Z. Pénzváltó, C. Pham, A.L. Koehne, A.C. Go, S.E. Anderson, P.M. Cala, and A.D. Borowsky. 2016. Glucose Uptake and Intracellular pH in a Mouse Model of Ductal Carcinoma In situ (DCIS) Suggests Metabolic Heterogeneity. *Front. Cell Dev. Biol.* 4:93. doi:10.3389/fcell.2016.00093.

Majdi, A., J. Mahmoudi, S. Sadigh-Eteghad, S.E.J. Golzari, B. Sabermarouf, and S. Reyhani-Rad. 2016. Permissive role of cytosolic pH acidification in neurodegeneration: A closer look at its causes and consequences. *J. Neurosci. Res.* 94:879–887. doi:10.1002/JNR.23757.

Martin, C., S.F. Pedersen, A. Schwab, and C. Stock. 2011a. Intracellular pH gradients in migrating cells. *Am. J. Physiol. - Cell Physiol.* 300:490–495.

bioRxiv preprint doi: https://doi.org/10.1101/2021.06.04.447151; this version posted June 7, 2022. The copyright holder for this preprint (which was not certified by peer review) is the author/funder, who has granted bioRxiv a license to display the preprint in perpetuity. It is made available under aCC-BY-NC-ND 4.0 International license.

1022 doi:10.1152/AJPCELL.00280.2010.

1023 Martin, C., S.F. Pedersen, A. Schwab, and C. Stock. 2011b. Intracellular pH gradients in

1024 migrating cells. *https://doi.org/10.1152/ajpcell.00280.2010*. 300:490–495.

1025 doi:10.1152/AJPCELL.00280.2010.

1026 Mirkka Koivusalo, Christopher Welch, Hisayoshi Hayashi, Cameron C. Scott, Moshe

1027 Kim, Todd Alexander, Nicolas Touret, Klaus M. Hahn, and S.G. 2010. Amiloride

1028 inhibits macropinocytosis by lowering submembranous pH and preventing Rac1

1029 and Cdc42 signaling. *J. Cell Biol.* doi:10.1083/jcb.200908086.

1030 Putney, L.K., and D.L. Barber. 2003. Na-H Exchange-dependent Increase in

1031 Intracellular pH Times G2/M Entry and Transition. *J. Biol. Chem.* 278:44645–

1032 44649. doi:10.1074/jbc.M308099200.

1033 Rajal, A.G., K.A. Marzec, R.A. McCloy, M. Nobis, V. Chin, J.F. Hastings, K. Lai, M.

1034 Kennerson, W.E. Hughes, V. Vaghjiani, P. Timpson, J.E. Cain, D.N. Watkins, D.R.

1035 Croucher, and A. Burgess. 2021. A non-genetic, cell cycle-dependent mechanism

1036 of platinum resistance in lung adenocarcinoma. *Elife*. 10. doi:10.7554/ELIFE.65234.

1037 Reshkin, S.J., A. Bellizzi, S. Caldeira, V. Albarani, I. Malanchi, M. Poignee, M. Alunni-

1038 Fabbroni, V. Casavola, and M. Tommasino. 2000. Na + /H + exchanger-dependent

1039 intracellular alkalinization is an early event in malignant transformation and plays an

1040 essential role in the development of subsequent transformation-associated

1041 phenotypes. *FASEB J.* 14:2185–2197. doi:10.1096/fj.00-0029com.

1042 Schatten, G., T. Bestor, R. Balczon, J. Henson, and H. Schatten. 1986. Intracellular pH

1043 Shift Initiates Microtubule-Mediated Motility during Sea Urchin Fertilization. *Ann. N.*

1044 *Y. Acad. Sci.* 466:940–944. doi:10.1111/J.1749-6632.1986.TB38480.X.

bioRxiv preprint doi: https://doi.org/10.1101/2021.06.04.447151; this version posted June 7, 2022. The copyright holder for this preprint (which was not certified by peer review) is the author/funder, who has granted bioRxiv a license to display the preprint in perpetuity. It is made available under aCC-BY-NC-ND 4.0 International license.

1045 Sellier, C., J.F. Bodart, S. Flament, F. Baert, J. Cannon, and J.P. Vilain. 2006.
1046 Intracellular acidification delays hormonal G2/M transition and inhibits G2/M
1047 transition triggered by thiophosphorylated MAPK in xenopus oocytes. *J. Cell.*
1048 *Biochem.* 98:287–300. doi:10.1002/jcb.20764.
1049 Sergeeva, T.F., M. V. Shirmanova, O.A. Zlobovskaya, A.I. Gavrina, V. V. Dudenkova,
1050 M.M. Lukina, K.A. Lukyanov, and E. V. Zagaynova. 2017. Relationship between
1051 intracellular pH, metabolic co-factors and caspase-3 activation in cancer cells
1052 during apoptosis. *Biochim. Biophys. Acta - Mol. Cell Res.* 1864:604–611.
1053 doi:10.1016/j.bbamcr.2016.12.022.
1054 Siu, K.T., M.R. Rosner, and A.C. Minella. 2012. An integrated view of cyclin E function
1055 and regulation. *Cell Cycle*. 11:57–64. doi:10.4161/cc.11.1.18775.
1056 Taylor, I.W., and P.J. Hodson. 1984. Cell cycle regulation by environmental pH. *J. Cell.*
1057 *Physiol.* 121:517–525. doi:10.1002/jcp.1041210310.
1058 Trotter, E.W., and I.M. Hagan. 2020. Release from cell cycle arrest with Cdk4/6
1059 inhibitors generates highly synchronized cell cycle progression in human cell
1060 culture. *Open Biol.* 10:200200. doi:10.1098/RSOB.200200.
1061 Watanabe, K., M.S. Hamaguchi, and Y. Hamaguchi. 1997. Effects of Intracellular pH on
1062 the Mitotic Apparatus and Mitotic Stage in the Sand Dollar Egg. *Cytoskeleton*.
1063 37:263–270. doi:10.1002/(SICI)1097-0169(1997)37:3.
1064 Weiß, I., and J. Bohrmann. 2019. Electrochemical gradients are involved in regulating
1065 cytoskeletal patterns during epithelial morphogenesis in the Drosophila ovary. *BMC*
1066 *Dev. Biol.* 19. doi:10.1186/s12861-019-0203-y.
1067 White, K.A., B.K. Grillo-Hill, and D.L. Barber. 2017a. Cancer cell behaviors mediated by

bioRxiv preprint doi: https://doi.org/10.1101/2021.06.04.447151; this version posted June 7, 2022. The copyright holder for this preprint (which was not certified by peer review) is the author/funder, who has granted bioRxiv a license to display the preprint in perpetuity. It is made available under aCC-BY-NC-ND 4.0 International license.

dysregulated pH dynamics at a glance. *J. Cell Sci.* 130:663–669. doi:10.1242/jcs.195297.

White, K.A., D.G. Ruiz, Z.A. Szpiech, N.B. Strauli, R.D. Hernandez, M.P. Jacobson, and D.L. Barber. 2017b. Cancer-associated arginine-to-histidine mutations confer a gain in pH sensing to mutant proteins. *Sci. Signal.* 10. doi:10.1126/scisignal.aam9931.